Modeling of Sorption Enhanced Steam Methane Reforming (SE-SMR) in an Adiabatic Packed Bed Reactor by using Different Sorbents

Submitted by

Muhammad Mateen

2016-MS-CH-10

Under supervision of

Dr. Syed Zaheer Abbas

Department of Chemical Engineering

University of Engineering and Technology, Lahore

Modeling of Sorption Enhanced Steam Methane Reforming (SE-SMR) in an adiabatic packed bed reactor by using different sorbents

This thesis is submitted to the department of chemical engineering, University of Engineering and Technology, Lahore for the partial fulfillment of the requirement for the Master of Science in CHEMICAL ENGINEERING

Approved on: _____

Signature: _____
Dr. Syed Zaheer Abbas
Supervisor/internal examiner

Signature: _____
Dr. Hamid Sattar
External examiner

Signature: _____
Prof. Dr. –Ing. Naveed Ramzan
Chairman

Signature: _____
Prof. Dr. Nadeem Feroze
Dean, Faculty of Chem., Met., & Polymer Engg.

Department of Chemical Engineering

University of Engineering and Technology, Lahore

DEDICATION

To my family, my friends, and my teachers without whose love and prayers this Research Thesis could not have been accomplished.

ACKNOWLEDGEMENTS

First and foremost, my due thanks to my supervisor Dr. Syed Zaheer Abbas. He was the great source of inspiration throughout the journey of this Research. His efforts and valuable suggestions are truly commendable. They gave me insights to think in an entirely different way to solve complex problems.

The following are also gratefully acknowledged: to the technical support of Dr. Zainab in CEA, the University of Engineering and technology (UET) Lahore, Prof. Mojtaba Gadhiri and University of Leeds, for access to the license for gPROMS modelbuilder.

ABSTRACT

One-dimensional heterogeneous model for sorption enhanced steam methane reforming (SE-SMR) process is developed for an adiabatic packed bed reactor and implemented this mathematical model in gPROMS Modelbuilder®. The reactor model is based on both gas and solid, mass and energy transfer principles along with the empirical correlations. The kinetic equations for CaO, lithium zirconate (LZC) and hydrotalcite (HTC) published in literature were used in the model. The performance of SE-SMR process is modelled to find the optimum operational conditions of temperature, pressure, steam to carbon ratio (S/C) and gas mass flow velocity (G_s). Concept of pre-breakthrough curve of these sorbents were studied using the transient temperature profiles. In the present work, low pressure (3 – 11 bar) is used for the SE-SMR process. The sensitive analysis was carried out by changing the operational parameters like temperature, pressure, S/C and G_s to study the CH_4 conversion, H_2 purity and yield, and CO_2 capture efficiency during the SE-SMR process. The simulation results were also compare with the equilibrium results generated through chemical equilibrium and application (CEA) software. It was concluded from the analysis that 82% CH_4 conversion and 85% H_2 purity can be achieved at 900 K, 3 bar, 3.5 $kgm^{-2}s^{-1}$ and S/C of 3.0 by using CaO sorbent. LZC and HTC gave high CH_4 conversion, 91.3 and 92.6% respectively, and H_2 purity 94.08 and 95.7% respectively. HTC gave more CH_4 conversion enhancement (C_F) than CaO and LZC, but with slow capture kinetics. In case of HTC, 5 bar, 900 K, and S/C of 3.0 gave 118% C_F

Table of Contents

DEDICATION iii

ACKNOWLEDGEMENTS iv

ABSTRACT v

LIST OF FIGURES vii

LIST OF TABLES viii

NOMENCLATURE ix

Chapter 1 LITERATURE SURVEY 1

Chapter 2 MATHEMATICAL MODELLING 5

2.1 SE-SMR kinetics 5

Chapter 3 RESULTS AND DISCUSSION 9

3.1 Model validation 9

3.2 Methodology of thermodynamic analysis 11

3.3 Analysis of temperature profile 11

3.4 Sensitivity analysis 12

3.4.1 Effect of temperature 12

3.4.2 Effect of pressure 16

3.4.3-Effect of G_s 19

3.4.4-CH_4 conversion enhancement factor (C_F) 21

3.5-Comparison of sorbent capacities 22

Chapter 4 CONCLUSION 23

References: 24

Appendix A: SMR and sorbent kinetic data 27

Appendix-B Empirical correlations 29

Appendix C: Rate equations for component ‘i’ 30

LIST OF FIGURES

Figure 3.1: Comparison of experimental and simulated extent of reaction (x) of CO2 sorption by using LZC at 848 K and 0.5 - 1 bar. Dots are the experimental data and solid lines are the outputs of our modelling work……..…….19

Figure 3.2: The effect of CO_2 partial pressure on the sorption capacity (mol kg^{-1}) of HTC under different temperature (673 – 753 K) conditions. Dots are the experimental data and solid lines are the outputs of our modelling work……20

Figure 3.3: Temperature profile of (a) CaO at 900 K, 3 bar, S/C of 3.0, and G_s of 3.5 $kgm^{-2}s^{-1}$ (b) LZC at 950 K, 10 bar, S/C of 3.0 and G_s of 2.5 $kgm^{-2}s^{-1}$ (c) HTC at 900 K, 5 bar, S/C of 3.0 and G_s of 0.5 $kgm^{-2}s^{-1}$……21

Figure 3.4: The effect of temperature on (a) CH_4 conversion (%), (b) H_2 yield (%), (c) H_2 purity (%) and (d) CO_2 capture efficiency (%) at 3 bar, S/C of 3.0 and 3.5 $kgm^{-2}s^{-1}$ by using CaO sorbent……..……23

Figure 3.5: The dynamic effect of temperature on the rate of carbonation ($mol_{CO2}/kg_{sorbent}$) of CaO sorbent at 3 bar, 3.5 $kgm^{-2}s^{-1}$ and S/C of 3.0…….24

Figure 3.6: The effect of temperature on (a) CH_4 conversion, (b) H_2 yield (wt. % of CH4), (c) H_2 purity (%) and (d) CO_2 capture efficiency at 10 bar, S/C of 3.0 and 2.5 $kgm^{-2}s^{-1}$ by using LZC sorbent…….….25

Figure 3.7: The effect of pressure on CH_4 conversion, H_2 yield (wt. % of CH_4), H_2 purity and CO_2 capture efficiency using (a) CaO, (b) LZC and (c) HTC at the optimum temperatures, S/C of 3.0 and sorbent/carbon of 1……...……27

Figure 3.8: The effect of pressure on the rate of SMR reaction (R1) and rate of carbonation by using (a) CaO at 900 K, S/C of 3.0 and G_s of 3.5 $kgm^{-2}s^{-1}$, (b) LZC at T = 950 K, S/C of 3.0 and G_s of 2.5 $kgm^{-2}s^{-1}$ and (c) HTC at 900 K, S/C of 3.0 and G_s of 0.5 $kgm^{-2}s^{-1}$……..…..28

Figure 3.9: The effect of G_s on the H_2 and CO_2 molar composition (dry basis) by using (a) CaO at 900 K, S/C of 3.0 and 3 bar, (b) LZC at 950 K, S/C of 3.0 and 10 bar and (c) HTC at 900 K, S/C of 3.0 and 5 bar…….29

Figure 3.10: CO_2 adsorb concentration using (a) CaO at 900 K, S/C of 3.0, 3 bar and Gs of 3.5 $kgm^{-2}s^{-1}$, (b) LZC at 950 K, S/C of 3.0,10 bar, and Gs of 2.5 $kgm^{-2}s^{-1}$ and (c) HTC at 900 K, S/C of 3.0, 5 bar and Gs of 0.5 $kgm^{-2}s^{-1}$……...30

LIST OF TABLES

Table 2.1: The parameters and operating conditions used in the modelling of SE-SMR reactor……...16

Table 2.2: SE-SMR reactor modelling equations…….....17

Table-3.1: The effect of temperature on CH_4 conversion, H_2 yield (wt. % of CH_4), H_2 purity and CO_2 capture efficiency at 5 bar, S/C of 3.0 and 0.5 $kgm^{-2}s^{-1}$ using HTC as a sorbent……..26

Table 3.2: The effect of S/C on C_F using different sorbents…….30

NOMENCLATURE

a_v	Interfacial area per unit volume, m^2m^{-3}
b_{CO2}	Temperature dependent Langmuir parameter, kPa^{-1}
$b_{CO2, ref}$	Temperature dependent Langmuir parameter at reference conditions, kPa^{-1}
C_i	Concentration of component i, mol m^{-3}
$C_{i,in}$	Concentration of component i at inlet, mol m^{-3}
$C_{i,o}$	Concentration of component i at t=0, mol m^{-3}
$C_{i,s}$	Concentration of component i on solid surface, mol m^{-3}
C_{pg}	Heat capacity of gas, J $kg^{-1}K^{-1}$
$C_{p,bed}$	Heat capacity of bed, J $kg^{-1}K^{-1}$
D_i	Effective diffusion coefficient, m^2 s^{-1}
D_m	Average molecular diffusivity, m^2 s^{-1}
d_P	Particle diameter of catalyst, m
D_p	Pore diffusion coefficient, m^2 s^{-1}
D_z	Axial dispersion coefficient, m^2 s^{-1}
E_j	Activation energy of reaction j, J mol^{-1}
E_{ad}	Activation energy of sorbents, J mol^{-1}
C_F	Conversion enhancement factor (%)
G_s	Gas mass flow velocity, kg m^{-2} s^{-1}
h_f	Heat transfer coefficient, W m^{-2} s^{-1}
$J_{D,i}$	Chilton-Colburn j-factor for mass transfer
J_H	Chilton-Colburn j-factor for heat transfer

k	Thermal conductivity, W m^{-1} K^{-1}
k_{eff}	Effective thermal conductivity, W m^{-1} K^{-1}
$k_{g,i}$	Gas to solid mass transfer coefficient of component i, m^3 $m^{-2}s^{-1}$
K_i	Sorption constant of species i
k_j	Kinetic constant of reaction j
$K_{o,i}$	Reference sorption constant of species i
K_j	Equilibrium constant of reaction j
k_z	Axial thermal conductivity, W m^{-1} K^{-1}
L	Length of reactor bed, m
m_{CO2}	Maximum sorption capacity for HTC, mol kg^{-1}
p_i	Partial pressure of specie i, bar
P	Total pressure, bar
p_i^{feed}	Partial pressure of component i in feed, bar
P^o	Pressure at z=0, bar
P_{in}	Inlet pressure of the feed, bar
P_r	Prandtl number
q_{CO2}	concentration of CO_2 on sorbent, mol kg^{-1}
$q_{CO2,\ max}$	Maximum carbonation conversion, mol kg^{-1}
R, R_g	Ideal gas constant, J $mol^{-1}K^{-1}$
r_i	Rate of formation of component i, mol $kg_{cat}^{-1}s^{-1}$
r_{ads}	Rate of sorption of CO_2, mol $kg^{-1}s^{-1}$
R_e	Reynolds number
R_j	Rate of reaction j, mol $kg_{cat}^{-1}s^{-1}$

S_{ci}	Schmidt's number
T	Temperature within reactor, K
T_{in}	Inlet temperature, K
T_s	Temperature of catalyst particles, K
$T_{s,o}$	Temperature of solid particles at 't=0', K
$u_{s,}$ v	Superficial velocity, m s^{-1}
X_{max}	Maximum fractional carbonation conversion of CaO
X_{CH4}	Fractional conversion of CH_4
x	Extent of reaction
ΔH_{rex}	Heat of reaction at standard conditions, J mol^{-1}
ΔH_{ads}	Heat of sorption reaction at standard conditions, J mol^{-1}
ΔP	Pressure drop across the bed reactor, bar
Greek Letters	
Ω	Denominator term in the reaction kinetics
λ_z^f	Effective thermal conductivity, W m^{-1} K^{-1}
λ_g	Average gas thermal conductivity, W m^{-1} K^{-1}
λ_s	Solid thermal conductivity, W m^{-1} K^{-1}
λ_z^o	Effective thermal conductivity of motionless fluid, W m^{-1} K^{-1}
ρ_f	Density of fluid, kg m^{-3}
ρ_{cat}	Density of catalyst, kg m^{-3}
ρ_{ad}	Density of sorbent, kg m^{-3}
η_j	Effectiveness factor
Φ_{ij}	Stoichiometric coefficient

μ_g	Viscosity of gas, Pa.s
υ	Ratio of amount of catalyst to amount of sorbent

Chapter 1 LITERATURE SURVEY

The ever-increasing energy demand, throughout the world together with global climate change, encourages the researchers to develop an innovative and sustainable technology for the energy production. Currently, most of the energy demand is accomplished through the burning of fossil fuels (86%); primarily from petroleum and natural gas (NG). Unfortunately, the burning of fossil fuels emits carbon dioxide (CO_2) and other various anthropogenic pollutants such as NO_x, SO_x and volatile organic compounds (VOCs), which ultimately contribute towards greenhouse gas (GHG) emissions and air pollution [1]. Over the past decade, fossil fuels account for 75% of CO_2 emissions in the atmosphere [2]. Among several different resources, hydrogen (H_2) is the most reliable and potential alternative energy carrier. H_2 is considered as a clean source of energy as the burning of H_2 only produces water (H_2O) as the byproduct [3]. H_2 is an important raw material used in the manufacturing of various commodity chemicals such as ammonia and methanol as well as in the petroleum industry [4]. The portion of H_2 consumed in ammonia and methanol production is 61% and 9% respectively [1]. The major technologies used for the production of H_2 are steam methane reforming (SMR), partial oxidation (POx), steam iron process, thermal deposition and electrolysis [1].

The SMR process is the most widely used technology for the commercial production of H_2 since 1930 [5]. More than 40% of world's H_2 production comes through the SMR process [1]. United States is producing about 95% of their total H_2 through SMR process [6]. The conventional SMR process usually carried out under high temperature (1073 – 1273 K) and pressure (20 – 35 bar) conditions in the presence of reforming catalyst (mostly Ni based) to convert methane (CH_4) into H_2, CO and CO_2 as shown in the SMR reaction (R1) and global SMR reaction (R2) [3].

$$CH_{4(g)} + H_2O_{(g)} \leftrightarrow CO_{(g)} + 3H_{2(g)} \qquad \Delta H^0_{298K} = 206.2 \text{ kJ mol}^{-1}_{CH_4} \qquad \text{(R1)}$$

$$CH_{4(g)} + 2H_2O_{(g)} \leftrightarrow CO_{2(g)} + 4H_{2(g)} \qquad \Delta H^0_{298K} = 165 \text{ kJmol}^{-1}_{CH_4} \qquad \text{(R2)}$$

The excess steam then reacts with CO in a water gas shift (WGS) reactor by the following WGS reaction (R3) to further maximize the H_2 yield (wt. % of CH_4) [7].

$$CO_{(g)} + H_2O_{(g)} \leftrightarrow CO_{2(g)} + H_{2(g)} \qquad \Delta H^0_{298K} = -41.2 \text{ kJmol}^{-1}_{CO} \qquad \text{(R3)}$$

The reforming and WGS are reversible reactions and are equilibrium limited due to the thermodynamic constraints and it is impossible to attain complete conversion of CH_4 and CO in a single reactor [8][3]. Further, the overall SMR process is relatively complex and highly endothermic in nature and it uses expensive alloy reformer tubes. Moreover, one ton of H_2 produced through SMR process releases approximately 8 ton of CO_2 into the atmosphere [9]. This excessive release of CO_2 gives overall low H_2 selectivity and low H_2 yield (wt. % of CH_4) [10]. The CO_2 is further removed by using ammine scrubbing and then H_2 is purified up to 99% using pressure swing sorption (PSA), but roughly 20% of H_2 is lost during PSA operation [7], [11].

These drawbacks of SMR process stimulated the researchers to develop more environmental friendly and less energy intensive processes for the production of H_2. One such innovative

technology uses sorbents during the SMR reaction for in-situ CO_2 capturing, while producing H_2 enriched gas (up to 97% dry basis) in a single reactor [11]. This process is called sorption enhanced steam methane reforming (SE-SMR). In SE-SMR process, reforming reactions (R1 & R2), WGS (R3) and sorption reaction (R4) takes place at the same time in a single packed bed reactor [12]. According to Le-chatleir's principle, the CO_2 removal will shift the overall reforming process towards more H_2 production [11]. As a result, high CH_4 conversion (%) can be achieved with almost complete conversion of CO to CO_2 [6]. The CO_2 sorption reaction is given as;

$$\mathrm{CO_{2(g)}} + \varepsilon_{(s)} \rightarrow \mathrm{CO_2}\varepsilon_{(s)}$$
(R4)

Where, $\varepsilon_{(s)}$ is CO_2 sorbent. The overall SE-SMR reaction would become;

$$\mathrm{CH_{4(g)}} + 2\mathrm{H_2O_{(g)}} + \varepsilon_{(s)} \leftrightarrow \mathrm{CO_2}\varepsilon_{(s)} + 4\mathrm{H_{2(g)}}$$
(R5)

The sorption of CO_2 is an exothermic process in which equilibrium capacity decreases with increase in temperature. The inclusion of exothermic calcined reaction forms the overall SE-SMR process essentially thermo-neutral and no extra energy is required during the SE-SMR process [13]. Moreover, the use of sorbents allows us to operate at comparatively low temperatures (~873 K) than conventional SMR process (950 – 1200 K). The use of low temperatures (~873 K) in SE-SMR process encourages the researchers to use less costly alloy reformer tubes [11]. The regeneration of sorbent releases fairly pure CO_2 which could be sequestered or stored in deep ocean reserves, depleted oil and gas reserves or in saline aquifers [14], [15]. The SE-SMR process needed most of the energy at the stage of regeneration, which is still 20-25 % less than the conventional SMR process [2].

A lot of research work has been conducted on experimentation and modeling of SE-SMR process [2], [3], [14]. Various sorbents such as zeolites, activated carbon, metallic oxides, dolomite, hunatite and hydrotalcite (HTC) can be used to capture CO_2. Zeolites and activated carbon show good CO_2 capturing capacities, for example, the capacity of 13X (linde, union carbide) zeolite has been measured as 4 moles CO_2 $kg^{-1}_{zeolite}$ at 300 K. Activated carbon has capacity about 1.5 - 2.5 moles CO_2 $kg^{-1}_{activated\ carbon}$ at 300 K. But, at high temperatures (> 873 K), their capacities decline rapidly [16]. The problem with SE-SMR process is that it operates at relatively high temperature (~873 K) which urges us to use selective sorbents that could work at around 873 K without having considerable effect on their capacities. The sorbent should also possess some noble qualities like fast kinetics, suitable thermodynamics, and high capacities at several sorption-regeneration cycles [17][18]. Further, the sorbent should be easily regenerated and available at low cost [19]. The metal oxides such as CaO, lithium oxides, shows good capacities and kinetics at high temperatures (>723 K). HTC can operate at high temperatures without considerable effect in sorption kinetics but the CO_2 absorption capacity is comparatively low as compare to other sorbents [20].

Lot of work has been done in SE-SMR process using CaO as sorbent. Williams [21] demonstrated that the use of lime could produce relatively pure H_2 (98%) by capturing CO_2. Lee et.al. [22] performed SE-SMR process using CaO at 873 – 1023 K. They showed that maximum uptake of CO_2 was found to be 5.09 mol_{CO2} kg^{-1}_{CaO} at 1023 K and 3 bar. Harrison et al. [23] investigated H_2 production via the WGS reaction (R3) using dolomite as a CO_2 sorbent at 773 – 873 K. The total concentration of CO_2 at the outlet was 50 ppm at most favorable conditions of 823 K and 15 bar. Abbas et al. [2] developed the 1-D heterogeneous mathematical model for the SE-SMR process using CaO as sorbent. The effect of different operational parameters such as temperature, pressure, S/C and G_s on the purity and yield of H_2 (wt. % of CH_4) , CO_2 capture efficiency and CH_4 conversion was studied and also validated the results against the equilibrium data and the modeling results taken from Fernandez et al. [3] They observed CH_4 conversion and H_2 purity up to 65% and 85% respectively at optimum operating conditions (923K, 30 bar and S/C of 3). CaO shows good sorption capacity. The stoichiometric sorption capacity of CaO is 0.79 g_{CO2} $g_{sorbent}^{-1}$ [6]. Unfortunately, the stability of CaO upon multiple carbonation – recarbonation cycle is the main concern. Dolomite retained about 60% of its initial capacity after 45 cycles, whereas CaO retained 40% of its initial capacity after 45 cycles [7][6]. The rapid decrease in stability is mainly due to the formation of layer of calcium carbonate ($CaCO_3$) on the surface of CaO sorbent during the multiple carbonation – recarbonation cycles [24]. To address this issue, researchers have tried to dope CaO with inert compounds such as Al_2O_3, MgO, and $Ca_{12}Al_{14}O_{33}$. Miaomiao et al. [25] doped CaO with calcium and aluminum precursors. They investigated $CaO - Ca_9Al_6O_{18}$ sorbent and found that it can retain 83% of its initial capacity after 50 carbonation – recarbonation cycles.

Recently, lithium and sodium oxides have been reported as promising candidates as sorbents for the SE-SMR process due to their reversible CO_2 capturing and favorable thermodynamics properties [26]. Lithium zirconate (LZC) has stoichiometric sorption capacity of 0.29 $g_{CO2}/g_{sorbent}$ and experimental capacity is 0.22 $g_{CO2}/g_{sorbent}$. LZC finds advantages over CaO in terms of low regeneration temperature [4]. Han et al. [4] simulate the performance of SE-SMR using LZC. They indicated that reaction rate determine step is surface controlled SE-SMR process. 87% of H_2 (dry basis) was found, but with longer fixed bed reactors. Halabi et al. [27] investigated the process of sorption enhanced auto thermal reforming (SE-AR) in a fixed bed reactor. The effect of mass and thermal dispersion, pressure drop and interfacial resistances was incorporated during SE-AR process. They examined two potential sorbents i.e. K-promoted HTC and LZC and observe their performance at 773 K and 4.47 bar using S/C of 6. LZC offered overall more CH_4 conversion (99.5%) and H_2 purity (99.5%, dry basis) as compare to K-promoted HTC with CH_4 conversion (85%) and H_2 purity (96%, dry basis). HTC is a complex compound consist of charged metallic and non-metallic ions, and has the ability to capture CO_2. It can operate under wet conditions and high temperatures [16]. Several K-promoted HTC have been tested and equilibrium CO_2 sorption capacity of 0.40 $mol_{CO2}/kg_{sorbent}$ over 6000 cycles have been found [7]. Ding et al. [16] developed dynamic model to study sorption and desorption of CO_2 on HTC. Langmuir model was assumed to be sufficiently dictate the sorption and desorption of CO_2 on HTC (at both dry and wet feed conditions). Sorption capacity was 10% more for wet feed conditions than for dry conditions but relatively slow deactivation was observed for wet feed conditions. They found sorption capacity of CO_2 on HTC based on wet feed to be 0.65 mol_{CO2}/kg

$_{sorbent}$ at 673 K. Ding et al. [28] also developed transient reactor model under non-isothermal, non-adiabatic and non-isobaric conditions. They showed that interparticle resistances and kinetic limitations of HTC could be overcome using high space time (τ_p). Aamir et al. [29] showed that HTC could be regenerated ,after CO_2 sorption, through temperature swing sorption (TSA) at 723 – 743 K. High sorption capacity (2.09 $mol_{CO2}/kg_{sorbent}$) of HTC doped with potassium (20 wt.%) was also measured by Joel et al. [8] at 3.1 bar.

Ochoa-Fernandez et al. [18] investigated the effect of various parameters on different sorbents using process design simulation software. They studied thermodynamic and kinetic behavior of different sorbents. Halabi et al. [27] studied the performance of LZC and HTC in the SE-AR process. Halabi et al. [30] also studied the kinetics and sorbent capacities of LZC and HTC using SE-SMR process. But, no work has been done on the mathematical modeling of SE-SMR process on 18wt.% NiO by using various sorbents available in the literature. Also, no research have been found to be conducted to find the ideal operating conditions like temperature, G_s, and S/C at low pressures (3 – 11 bar) for different sorbents (CaO, LZC and HTC) using SE-SMR process. To fill this gap, a one dimensional heterogeneous model of SE-SMR process is developed and implemented in gPROMS for the solution of equations. In this work, CaO, LZC, and HTC sorbents are used. The overall performance of the process is studies under the various operating conditions of temperature, pressure, S/C and gas mass flow velocity (G_s). The developed model is validated against the equilibrium data developed on an individual equilibrium software i.e. chemical equilibrium with application (CEA) and with the results of Ding et al.[16] and Ochoa-Fernandez et al [31] .

Chapter 2 MATHEMATICAL MODELLING

2.1 SE-SMR kinetics

In the modelling of SE-SMR reactor, the rate equations and kinetics data for the SMR process is taken from Xu et al. [32] as shown in Appendix A-1. This data includes the kinetics and equilibrium constants along with the reaction rate expressions. As in the SE-SMR process sorbent is added to capture CO_2 produced during the reforming process, the reaction between CO_2 and CaO is given as;

$$CaO_{(s)} + CO_{2(g)} \rightarrow CaCO_{3(s)} \qquad \Delta H^{0}_{298K} = -178.8\ \text{kJmol}^{-1}_{CaO}$$

(R6)

The overall SE-SMR reaction using CaO would become slightly exothermic in nature as shown below;

$$CH_{4(g)} + 2H_2O_{(g)} + CaO_{(s)} \leftrightarrow CaCO_{3(s)} + 4H_{2(g)} \qquad \Delta H^{0}_{298K} = -13.9\ \text{kJmol}^{-1}_{CaO}$$

(R7)

Many expressions have been published in the literature to explain the CO_2 capturing kinetics of CaO [3], [14], [22]. CaO is widely used in the literature because of its high sorption capacity and fast kinetics [33]. Different models have been adopted to express the kinetics of CaO. The selection of models greatly depends upon the experimental procedures and morphology of the sorbents. The conversion of CaO to $CaCO_3$ calculated from thermogravimetric analysis (TGA) usually varies from 60 to 100%. Pore blockage and buildup of solid $CaCO_3$ layer on surface of CaO sorbent affect the CaO conversion. Johnsen et al. [14] used energy dispersive X-ray spectroscopy together with scanning electron microscope (SEM) to investigate the concentration of oxygen at the outer surface of dolomite. The concentration of oxygen at the outer surface was twice as compare to the inner surface. They concluded that CO_2 does not react steadily over the entire surface of dolomite. To describe the carbonation kinetics, shrinking core model (SCM) was used by Johnsen et al [14]. Nikulshina et al. [34] analyzed the 500 ppm concentrated CO_2 (present in air) over CaO at 473 – 723 K in TGA to study the CO_2 capturing kinetics. They choose unreacted kinetic model (UKM) to precisely describe the capturing of CO_2 over CaO. Lee et al. [22] also used TGA to examine the carbonation conversion data over the temperature range of 923 – 1023 K. They also determined the maximum CaO conversion (X_{max}) by using different temperatures (873 – 1023 K). Rodrigues et al. [35] reported first order carbonation kinetics for the capturing of CO_2. The kinetic expression used by Rodrigues for CO_2 capturing over the active sites of CaO sorbent is used in this study and given in Appendix-A2.

The sorption of CO_2 over LZC is a highly exothermic reaction as indicated in R8.

$$Li_2ZrO_{3(s)} + CO_{2(g)} \rightarrow Li_2CO_{3(s)} + ZrO_{2(s)} \qquad \Delta H^{0}_{298K} = -160\ \text{kJmol}^{-1}_{Li_2ZrO_3} \qquad \text{(R8)}$$

The overall SE-SMR process using LZC is almost thermo-neutral with $\Delta H^{0}_{298K} = 5\ \text{kJmol}^{-1}_{Li_2ZrO_3}$. The high sorption capacity of LZC is the clear advantage for SE-SMR process, but Halabi et al. [30] reported overall slow carbonation kinetics. Ida et al. [36] found kinetics of gas phase reaction between CO_2 and LZC by using double shell unreacted core model. They

observe that the layer of Li_2CO_3 was produced over the inner layer of zirconium dioxide (ZrO_2) after the initial stages of carbonation reaction. Therefore, the diffusion of CO_2 into the Li_2CO_3 layer was determined as rate limiting step. Ochoa-Fernandez et al. [31] studied the properties of CO_2 capture over LZC by passing the mixture of CO_2 and argon (Ar) into the tapered-element oscillating microbalance reactor (TOEM). They used the extent of reaction (x) to describe the CO_2 capture properties over LZC. The kinetics proposed by Ochoa et al. [31] is used in this work and the rate equations are given in Appendix-A3.

K – HTC shows irreversible chemisorption of CO_2 over the fresh sorbent followed by reversible and weak physical sorption. The sorption of CO_2 above HTC is slightly exothermic with $\Delta H^0_{298K} = -17\ \text{kJmol}^{-1}_{\text{K-HTC}}$. Ding et al. [16] used Langmuir model to adequately describe the CO_2 sorption kinetics by using both dry and wet feed conditions. The sorption capacity was 10% more for wet feed conditions than for the dry feed conditions. They found sorption capacity of CO_2 on HTC (based on wet feed) to be $0.65 mol_{CO2}/kg_{\ sorbent}$ at 673 K. The linear driving force (LDF) model was found to be sufficient describing the intraparticle mass transfer process during carbonation reaction. The kinetic model of HTC along with effective mass transfer coefficient, Langmuir model parameter, and LDF model is presented in Appendix-A4.

Table 2.1: The parameters and operating conditions used in the modelling of SE-SMR reactor

Reactor bed characteristics and operating conditions	**Value**
Density of catalyst, ρ_{cat} [kg m^{-3}]	550
Density of bed, ρ_{bed} [kg m^{-3}]	1625
Specific heat of bed, $C_{p,bed}$ [J kg^{-1} K^{-1}]	980
Average gas viscosity, μ [kg m^{-1} s^{-1}]	1.8×10^{-4}
Steam to carbon ratio, S/C [-]	3
Particle diameter, d_p [m]	0.01
Bed porosity, ε_b [-]	0.5
Reactor length, L [m]	7
CaO density, $\rho_{ads,CaO}$ [kg m^{-3}]	1125
LZC density, $\rho_{ads,LZC}$ [kg m^{-3}]	596
HTC density, $\rho_{ads,HTC}$ [kg m^{-3}]	1300

2.2 Model description

To illustrate the physical and chemical behavior, 1-dimensional heterogeneous model is developed for the SE-SMR process by using mass and energy balance equations that account for both solid and gas phases. Dynamic packed bed reactor model is formulated due to the time dependent nature of sorption reaction (R4). The flow of gases in a reactor is assumed to be essentially ideal plug flow in nature and direction of flow of gases is supposed to be only in axial direction. Peclet number ($Pe = uL/D_e$) is considered to be greater than 800, so that the mixing of gases and variation of temperature and concentration across the radial direction of packed bed

reactor can be neglected. In order to take complete advantage from the exothermic nature of sorption reaction (R4), adiabatic nature of packed bed reactor is assumed. Fernandez et al. [3] suggested that adiabatic SE-SMR reactor gives shorter pre-breakthrough period as compare to non-adiabatic (quasi-isothermal) reactor. The adiabatic process also enhanced the energy efficiency of the reactor and it eliminated the need of heat transfer equipment for SE-SMR process [3]. Only CO_2 is considered to be adsorbed on the surface of sorbent while other components like CH_4, CO, H_2O, H_2, and N_2 are expected to be non-adsorbing species for the sorbent. Ideal gas behavior of gases, uniform size of the catalyst and sorbent throughout the reactor, and constant packed bed porosity is also assumed.

The parameters and operating conditions used during the modelling of SE-SMR reactor are tabulated in Table 2.1. Table 2.2 illustrates the mass and energy balances for component 'i' (i = CH_4, CO, CO_2, H_2, and H_2O) in both gas and solid phase. Where 'ε_b' is the bed porosity, 'ρ_g' and 'C_{pg}' are density and specific heat of gases, 'η_j' is the effectiveness factor. In the current model, $\eta_j$is assumed equal to 1 by neglecting diffusion resistance between gas and solid phases. Effect of the variation of temperature is also incorporated in the heat capacity of gases. The pressure drop in the bed of reactor is modified using Ergun's equation. The equations regarding calculations of physical properties like thermal conductivities, mass and heat transfer coefficient along with dimensionless numbers are presented in Appendix-B. Both mass and energy balances contain partial differential equations and algebraic equations. To solve these equations, initial and boundary conditions are also listed in Table 2.2. At the start of the reactor, initial concentration (C_i) should be set to zero, but this will make the SMR rates infinity. To avoid this problem, a very small initial concentration is set for H_2.

The model is implemented in gPROMs for the solution of the equations. To solve partial differential equations included in this model, a first order backward finite difference method (BFDM) was used. The reactor length (L) was discretized into 100 uniform intervals and results were reported after every 10 s.

Table 2.2: SE-SMR reactor modelling equations

Gas and solid phase material and energy balances.

$$\varepsilon_b\left(\frac{\partial C_i}{\partial t}\right) + \frac{\partial(uC_i)}{\partial z} + k_{g,i}a_v\left(C_i - C_{i,s}\right) = \varepsilon_b D_z \frac{\partial^2 C_i}{\partial z^2} \quad (1)$$

$$k_{g,i}a_v\left(C_i - C_{i,s}\right) = \upsilon\rho_{cat}r_i - (1-\upsilon)\,\rho_{ads}r_{ads} \quad (2)$$

$$\varepsilon_b\rho_g C_{pg}\left(\frac{\partial T}{\partial t}\right) + u\rho_g C_{pg}\frac{\partial(T)}{\partial z} = h_f a_v(T_s - T) + \lambda_z^f \frac{\partial^2 T}{\partial z^2} \quad (3)$$

$$\rho_{bed} C_{p,bed} \left(\frac{\partial T_s}{\partial t}\right) + h_f a_v (T_s - T)$$

$$= \upsilon \rho_{cat} \sum -\Delta H_{rxn,j}\, \eta_j R_j + (1 - \upsilon)\, \rho_{ads} \sum -\Delta H_{ads}\, r_{ads} \qquad (4)$$

Pressure drop calculations across the reactor bed;

$$\frac{\Delta P g_c}{L} = \frac{150}{d_p^2}\left[\frac{(1-\varepsilon)^2}{\varepsilon^3}\right]\mu u + \left(\frac{1.75}{d_p}\right)\left(\frac{1-\varepsilon}{\varepsilon^3}\right)\rho_g u^2 \qquad (5)$$

Boundary conditions

At the inlet of reactor i.e. z = 0

$C_i = C_{i,in}$; $T = T_{in}$; $T_s = T_{s,in}$; $P = P_{in}$

At the outlet of reactor i.e. z = L

$\frac{\partial C_i}{\partial z} = 0$; $\frac{\partial T}{\partial z} = 0$; $\frac{\partial T_s}{\partial z} = 0$

Initial condition

$C_i = C_{i,0}$; $T = T_o$; $T_s = T_{s,o}$; $q_{CO2} = 0$

Chapter 3 RESULTS AND DISCUSSION

3.1 Model validation

In our previous work [37], the SE-SMR process in an adiabatic packed bed reactor using CaO as sorbent is validated against the outcomes of CEA and literature data . To study the performance of SE-SMR process we used the industrial conditions for temperature, pressure and S/C .In the current work, we are using the same validated model to understand the performance of SE-SMR reactor under the low pressure conditions (3 – 11 bar) by using different (CaO, LZC and HTC) sorbents.

The extent of reaction (x) of CO_2 sorption using LZC as CO_2 sorbent is simulated and validated against the experimental outcomes of Ochoa-Fernandez et al. [31] Figure 3.1 shows the dynamic variation in the extent of reaction at various partial pressures of CO_2 (0.5, 0.7 and 1 bar). The values for kinetic parameters (k_{ad}, E_{ad}, T_o, and n) are taken from the literature and presented in Appendix A-3 [31]. At high p_{CO_2} (1 bar), the LZC sorbent approaches its saturation point quickly as compared to the low values of p_{CO_2} because CO_2 sorption on LZC favored under high pressure conditions. There is an excellent agreement observed between the modelling outputs and the experimental results available in the literature.

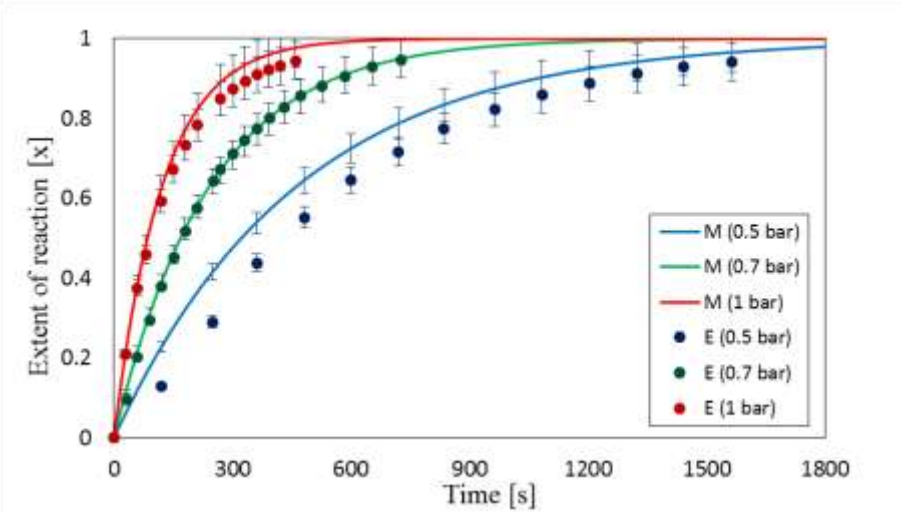

Figure 3.1: Comparison of experimental and simulated extent of reaction (x) of CO2 sorption by using LZC at 848 K and 0.5 - 1 bar. Dots are the experimental data and solid lines are the outputs of our modelling work.

At 150s, the simulated extent of reaction (x_M) for $p_{CO_2} = 1$bar is 0.673 ($uptake_{CO2}$/maximum $uptake_{CO2}$), whereas experimental extent of reaction (x_E) at 150s is 0.707. Similarly, the experimental and modeling data for the extent of reaction at $p_{CO_2} = 0.7$bar and 270s is 0.670 and 0.671 respectively. At p_{CO_2} = 0.5 bar, the x_E and x_M curves are less sharp and large time is required to saturate the LZC sorbent because the kinetics of LZC reported by Ochoa-Fernandez

et al [31] is of second order. They reported complex mechanism for CO_2 sorption on LZC and modeling equations that was used to describe CO_2 sorption experimentally indicated the second order reaction.

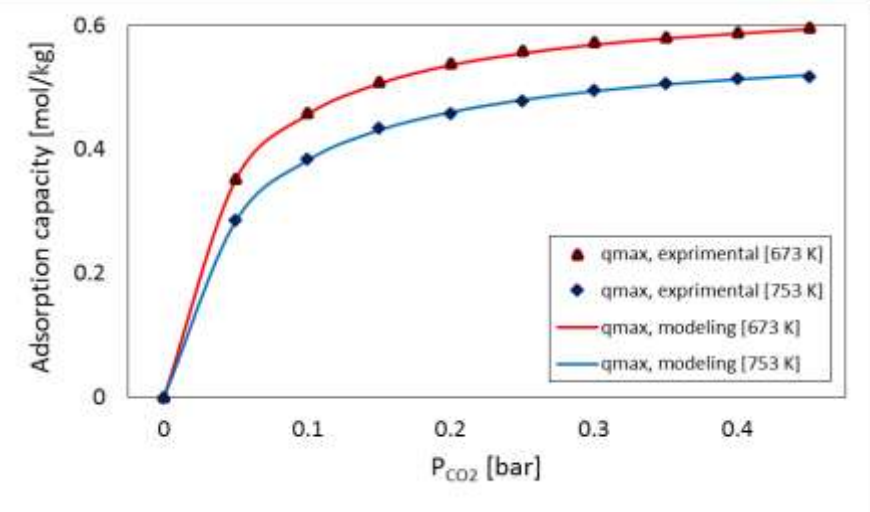

Figure 3.2: The effect of CO_2 partial pressure on the sorption capacity (mol kg-1) of HTC under different temperature (673 – 753 K) conditions. Dots are the experimental data and solid lines are the outputs of our modelling work.

The kinetics of HTC (Appendix A-4) used in this study are first validated by using the experimental data of Ding et al. [16]. The model is validated under both dry and wet feed conditions. As steam is used as reactant in SE-SMR process, only wet feed conditions are discussed here at under the operating conditions of 673 K and 753 K. Figure 3.2 shows the effect of p_{CO2} (0 – 0.45 bar) on the sorption capacity of HTC at 673 K and 753 K. The values for the model parameters like; pore diffusion coefficient (D_p), reference temperature (T_o) and heat of sorption (ΔH_{ads}) is taken from the literature [16]. The value of ΔH_{ads} is -10 kJ mol^{-1} and -17 kJ mol^{-1} for the dry and wet feed conditions respectively.

It can be seen in Figure 3.2 that both Langmuir isotherm curves show a sudden rise for 0 – 0.1 bar, which illustrates that sorption capacity of HTC is increased as the p_{CO_2} increased from 0 – 0.1 bar. At 673 K, Langmuir parameter ($b_{CO_2,ref}$) is 23.6 bar^{-1} and maximum sorption capacity (0.65 mol_{CO2}/kg_{HTC}) is used. At 673 K and 0.2 bar, the modeling and experimental value of sorption capacity is 0.536 and 0.539 mol_{CO2}/kg_{HTC} respectively. At 753 K and 0.2 bar p_{CO_2} , the modeling and experimental value of sorption capacity is 0.460 and 0.458 mol_{CO2}/kg_{HTC} respectively. An excellent agreement is observed between modeling and experimental values of sorption isotherm.

3.2 Methodology of thermodynamic analysis

An independent equilibrium based software, CEA by NASA, is used to calculate thermodynamic equilibrium composition of product gases by specifying the operating conditions of temperature and pressure. The CEA is based on minimization of Gibbs free energy. In this study, chemical equilibrium of SE-SMR process is calculated for CaO and LZC sorbents by specifying the different conditions of temperature, pressure, and S/C. The thermodynamic data (enthalpy, entropy, heat capacity and heat of formation) for LZC is taken from the literature [38], [39] and is inserted in CEA database (thermo.inp file). CH_4, CO, CO_2, H_2, H_2O, N_2, CaO, and $Ca(OH)_2$ is added in CEA. N_2 is added to calculate the total moles out. . The 'only' command is used to specify the possible products obtained from the SE-SMR process. The effect of temperature and pressure is studied by considering the reactor system at isobaric and isothermal conditions respectively. The effect of S/C is studied at equilibrium by keeping both pressure and temperature constant.

3.3 Analysis of temperature profile

The sorption of CO_2 over sorbents is exothermic in nature. This exothermic nature of sorption reaction (R4) causes a rise in the temperature of SE-SMR process from its initial (feed) temperature, depending on the quantity of heat (ΔH_{ads}) released by the sorbent. This rise in temperature will give transient temperature profile inside the reactor for different sorbents. Figure 3.3 (a – c) shows the transient temperature profiles of SE-SMR process using CaO, LZC and HTC as sorbents. Figure 3.3(a) presents the temperature profile, at the exit of reactor, using CaO as a sorbent at 900 K, 3 bar, S/C of 3.0 and G_s of 3.5 $kgm^{-2}s^{-1}$. During the initial stages (t = 0 – 200s), the temperature profile is almost steady.

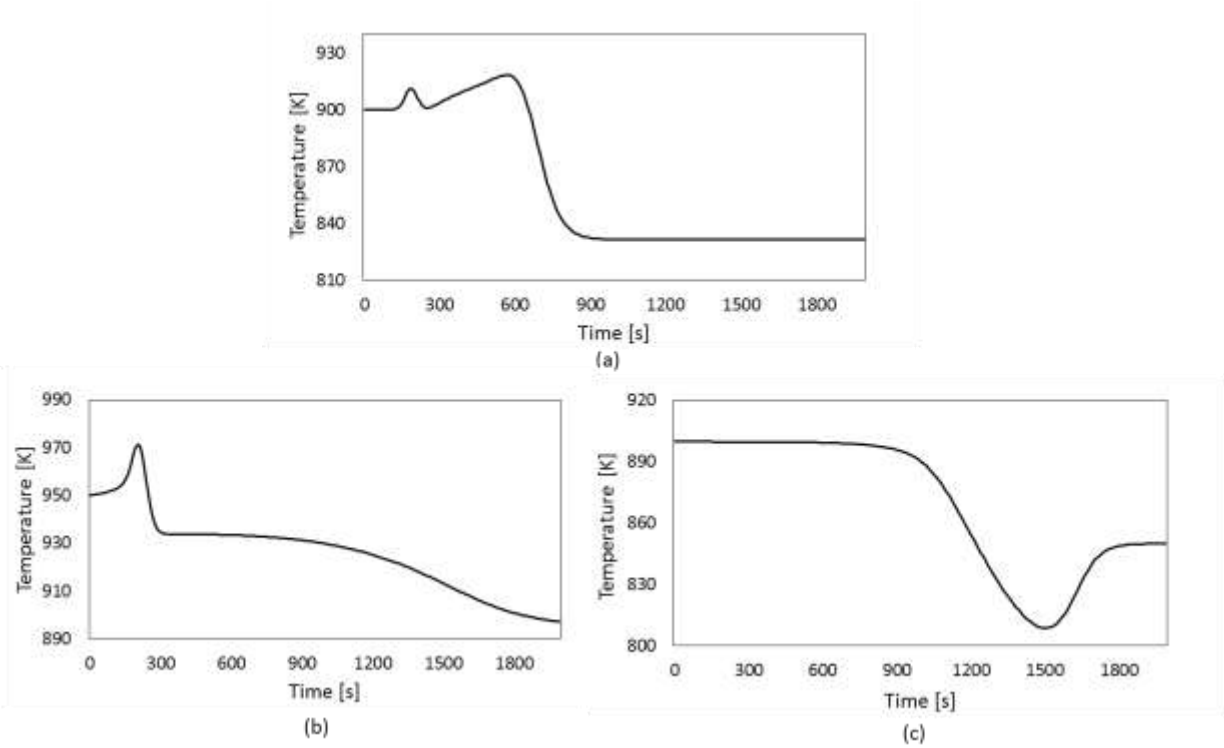

Figure 3.3: Temperature profile of (a) CaO at 900 K, 3 bar, S/C of 3.0, and Gs of 3.5 kgm-2s-1 (b) LZC at 950 K, 10 bar, S/C of 3.0 and Gs of 2.5 kgm-2s-1 (c) HTC at 900 K, 5 bar, S/C of 3.0 and Gs of 0.5 kgm-2s-1.

The heat supplied by the exothermic sorption reaction (R4) is fully utilized by the endothermic SMR reactions (R1 and R2), hence a steady uniform linear temperature profile is observed. Since, the overall SE-SMR process using CaO is slightly exothermic ($\Delta H^0_{298K} = -13.9\ kJmol^{-1}_{CaO}$), two peaks can be observed in the temperature profile (Figure 3.3(a)). The first rise in the temperature shows fast sorption at t = 200s. According to Le-chatleir principle, this rapid sorption of CO_2 will enhance the CH_4 conversion and will produce more H_2 and CO_2 at the outlet of the reactor. The more sorption of CO_2 results in continue rise in the temperature profile as can be seen from 280 – 690s (pre-breakthrough period). Once the sorbent is fully saturated a sharp decrease in temperature profile is observed from 690s – 910s (breakthrough period). After the breakthrough period (t > 910s), the SE-SMR process behaves similar to the SMR process as no CO_2 sorption is taking place and only the reforming (R1 and R2) and shift (R3) reactions are occurring within the reactor. The cut-off for the reactor bed should be somewhere in the breakthrough region where the optimal CH_4 conversion is achieved along with the optimal H_2 purity. It is actually the tradeoff between the overall CO_2 sorbent capacities used during the SE-SMR process and the optimal H_2 purity and CH_4 conversion achieved. Fernendes et al. [3] found the rise in temperature ($\Delta T_{rise} = T_{max} - T_{feed}$) during the SE-SMR process to be 32 K. In this study, ΔT_{rise} is 17.5 K. The low ΔT_{rise} is because the endothermic SMR process favors low pressure as described earlier. As a result, high CH_4 conversion (%) is achieved at low pressure conditions.

The temperature profiles for LZC and HTC is shown in Figure 3.3 (b) and (c) respectively. The pre-breakthrough period for LZC (t < 250s) is much smaller than the pre-breakthrough period in case of CaO (t < 690s). This indicates the less sorption capacity of LZC (5 $mol_{CO2}kg_{sorbent}^{-1}$) as compared to CaO (16.3 $mol_{CO2}kg_{sorbent}^{-1}$). The breakthrough period for LZC is last for 1870s, and the ΔT_{rise} for LZC is 20 K as compared to 17.5 K in case of CaO. The temperature profile is entirely different when HTC is used as a sorbent. There was no rise in the temperature observed for the HTC because of its low heat of sorption ($\Delta H^0_{298K} = -15\ kJmol^{-1}_{K-HTC}$). The overall SE-SMR process using HTC remains endothermic in nature. During the pre-breakthrough period, the time dependent temperature profile at the outlet of reactor using HTC remains steady. The long pre-breakthrough (t < 1040) curve for HTC is due to the low value of G_s (0.5 $kgm^{-2}s^{-1}$) used. The breakthrough period (t = 1040 – 1750 s) occurs where the curve starts bending. In, post breakthrough region, only SMR reaction is taking place.

3.4 Sensitivity analysis

3.4.1 Effect of temperature

The conventional SMR process is operated in fertilizer industries over the range of 1073 – 1273 K and 20 – 35 bar. Since, sorption of CO_2 and SMR is temperature sensitive process, the variation in temperature will definitely influence the SE-SMR process performance. Here, the performance of reactor is illustrated in terms of CH_4 conversion, H_2 yield, H_2 purity, CO_2 capture efficiency.

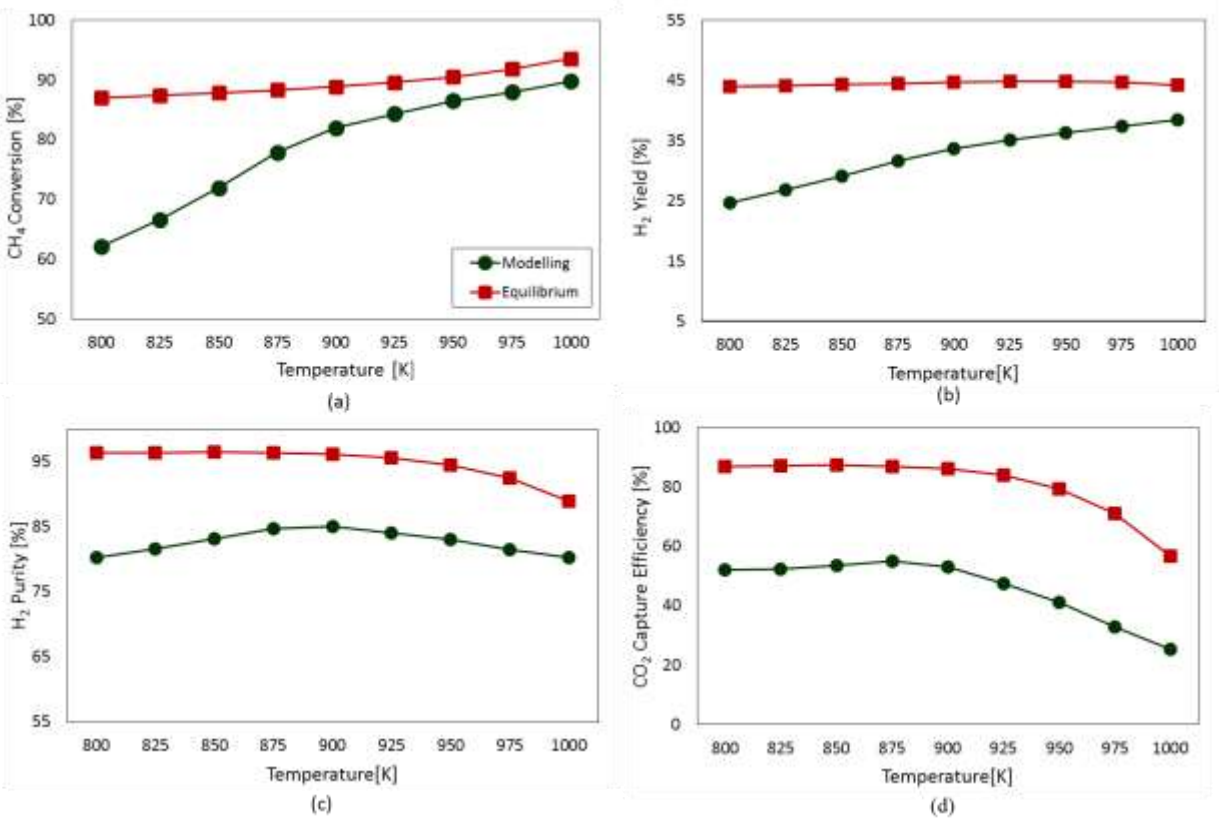

Figure 3.4: The effect of temperature on (a) CH_4 conversion (%), (b) H_2 yield (%), (c) H_2 purity (%) and (d) CO_2 capture efficiency (%) at 3 bar, S/C of 3.0 and 3.5 $kgm^{-2}s^{-1}$ by using CaO sorbent

Figure-3.4 (a) shows the effect of temperature on CH_4 conversion at 3.5 $kgm^{-2}s^{-1}$ and 3 bar, by using S/C of 3. At 800 K, the simulated CH_4 conversion (62.1%) is much lower as compared to the equilibrium results (86.9%) generated via CEA software as the SMR kinetics are not favorable at such low temperature (800 K). As, the temperature increases from 800 – 1000 K, the CH_4 conversion increases from 62.16 – 89.75 % and 86.98 – 93.57 % in case of simulation and equilibrium respectively.

At 900 K, we get 85% and 55% value of the H_2 purity and CO_2 capturing efficiency respectively in simulation. While the equilibrium values of H_2 purity and CO_2 capturing efficiency under the same temperature is 96.19 and 85.99 % respectively. At 1000 K, the simulation results give 89.7 % CH_4 conversion but the H_2 purity achieved at this temperature is 80.3%. This is due to very low CO_2 capture efficiency i.e. 25.37 % at such a high temperature. The low CO_2 capturing efficiency at 1000 K is mainly due to the ineffectiveness of carbonation reaction (R6) at such a high temperature and it is explained further in Figure 3.5.

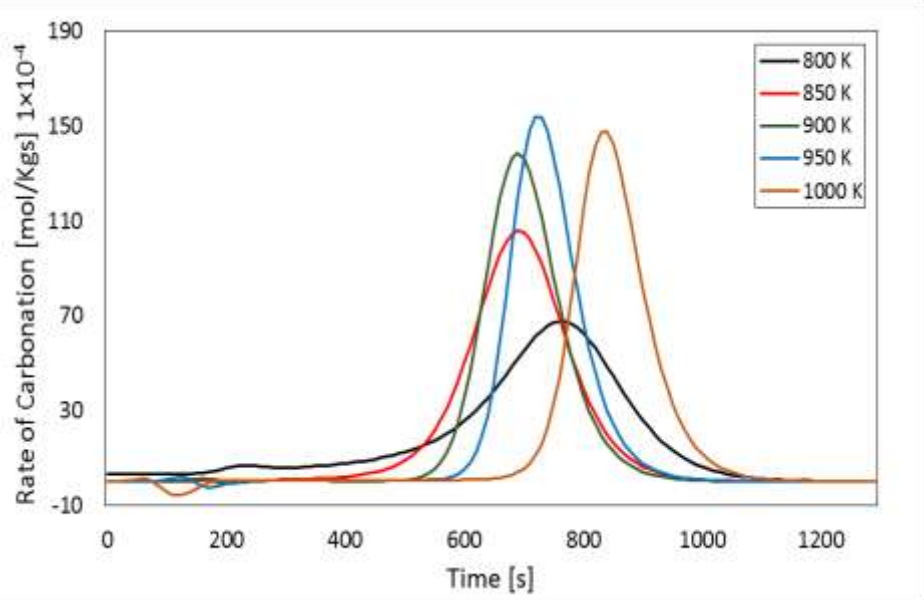

Figure 3.5: The dynamic effect of temperature on the rate of carbonation ($mol_{CO2}/kg_{sorbent}$) of CaO sorbent at 3 bar, 3.5 $kgm^{-2}s^{-1}$ and S/C of 3.0.

Figure 3.5 shows the effect of temperature on the rate of carbonation (r_{ads}) at 800 – 1000 K using CaO sorbent. The rate of carbonation increases as the temperature increases from 800 – 950 K. This shows the increase in temperature results in more capturing of CO_2 on the active sites of CaO sorbent. After 950 K, the r_{ads} decreases. At 800 K, the peak value for the r_{ads} is 6.8×10^{-3} mol $kg^{-1}s^{-1}$ as compared to 13.6×10^{-3} and 15.4×10^{-3} mol $kg^{-1}s^{-1}$ at 900 and 950 K respectively. The pre-breakthrough point at 800 K and 950 K is 780s and 730s respectively. This shows that CaO saturates quickly at 950 K than at 800 K.

Figure 3.6 shows the effect of temperature on CH_4 conversion, H_2 purity, H_2 yield (wt. % of CH_4) and CO_2 capturing efficiency at 10 bar and 3.5 $kgm^{-2}s^{-1}$ by using LZC as a sorbent. The CH_4 conversion increases with the increase in temperature and at 950 K and S/C of 3, 91.2% and 94% CH_4 conversion is achieved in case of modeling and equilibrium results respectively. At 975 K, H_2 purity and CO_2 capturing efficiency reach their maximum value of 95.5 % and 86.7% respectively. As temperature increases from 975 – 1000 K, the H_2 purity and CO_2 capturing efficiency decrease to 94.75% and 83.8% respectively.

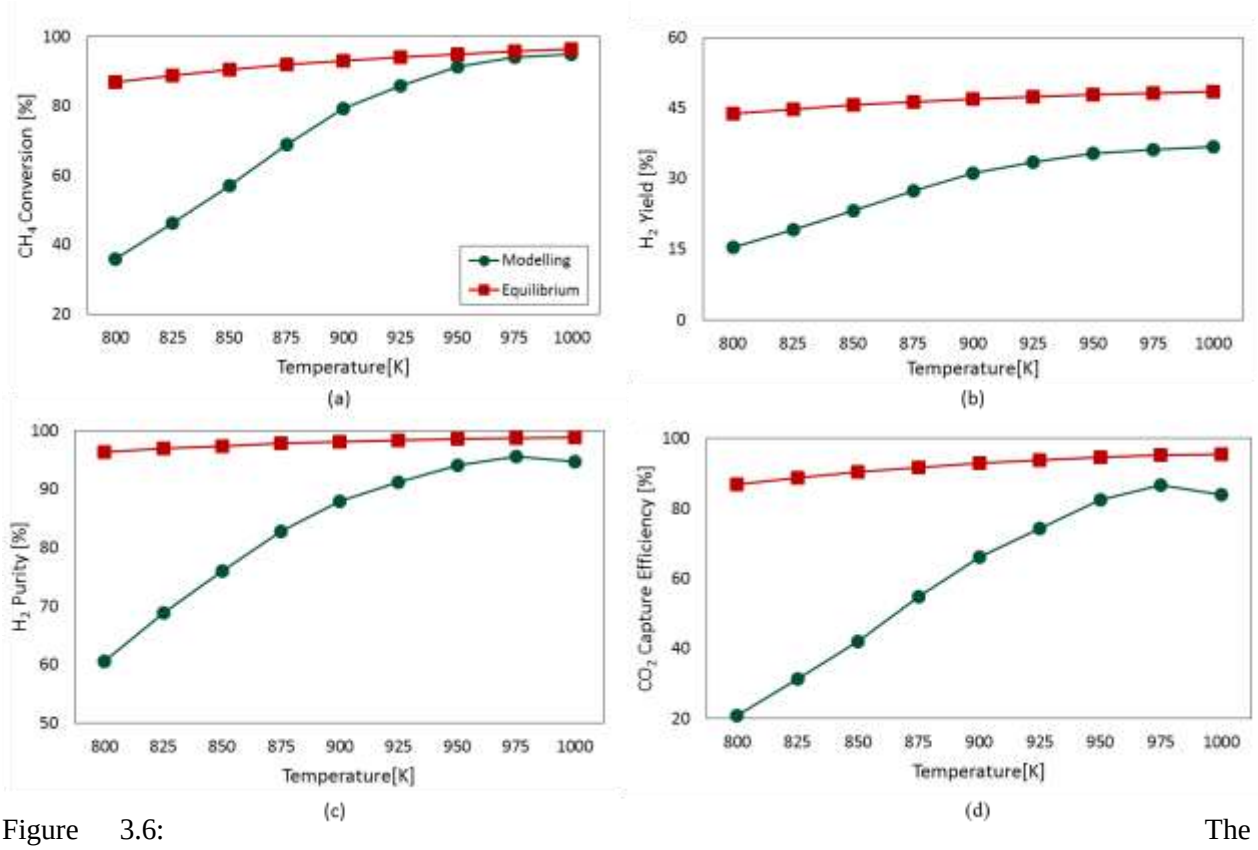

Figure 3.6: The effect of temperature on (a) CH_4 conversion, (b) H_2 yield (wt. % of CH4), (c) H_2 purity (%) and (d) CO_2 capture efficiency at 10 bar, S/C of 3.0 and 2.5 $kgm^{-2}s^{-1}$ by using LZC sorbent

Table 3.1 illustrates the effect of temperature on CH_4 conversion H_2 yield and purity, and CO_2 capturing efficiency using HTC at 5 bar, 0.5 $kgm^{-2}s^{-1}$ and S/C of 3. CH_4 conversion and H_2 yield increases continuously as the temperature increases from 800 – 1000 K. Initially, H_2 purity increases up to 94.4% at 900 K and then starts decreasing as the temperature increases from 900 – 1000 K. The drop in H_2 purity is due to the decrease in CO_2 capture efficiency as it can be seen in Table 3.1.

The selection of optimum temperature depends upon the overall performance of the sorbent in terms of CH_4 conversion, H_2 yield (wt. % of CH_4), H_2 purity and CO_2 capturing efficiency. 900 K is selected as an optimum temperature for CaO and HTC sorbents. 950 K is selected as the optimum temperature for LZC.

Table-3.1: The effect of temperature on CH_4 conversion, H_2 yield (wt. % of CH_4), H_2 purity and CO_2 capture efficiency at 5 bar, S/C of 3.0 and 0.5 $kgm^{-2}s^{-1}$ using HTC as a sorbent

Temperature [K]	**CH_4 conversion [%]**	**H_2 yield [wt. % of CH_4]**	**H_2 purity [%]**	**CO_2 capturing efficiency [%]**
800	60.19	23.25	81.01	56.84
825	70.18	27.07	86.43	66.34
850	78.78	30.36	90.35	74.32
875	86.53	33.32	93.48	81.58
900	90.11	34.77	94.44	83.77
925	91.11	35.28	94.29	83.07
950	91.37	35.48	93.98	82.00
975	92.17	36.02	93.26	79.38
1000	93.58	37.06	91.51	72.77

3.4.2 Effect of pressure

A lot of work has been done in the literature to investigate the performance of SE-SMR process under the high pressure conditions (20 – 40 bar) [2], [3], [14]. Since SMR operation is favorable at low pressure, it could be valuable to test SE-SMR model close to atmospheric conditions as high pressure conditions give low H_2 purity and CH_4 conversion. Kwang et al. [12] tested calcined arctic dolomite at low pressure condition (1 – 5 bar) and obtained 95% purity of H_2 (dry basis). The current model of SE-SMR is developed and simulated under low pressure conditions (3 – 11 bar) to find the best operating conditions for CaO, LZC and HTC sorbents.

In the previous section, optimum temperatures were selected for CaO, LZC and HTC. In this section, at the selected optimum temperatures, the optimum values for the pressure are investigated. Figure 3.7 illustrates the performance of CaO, LZC and HTC at low pressure

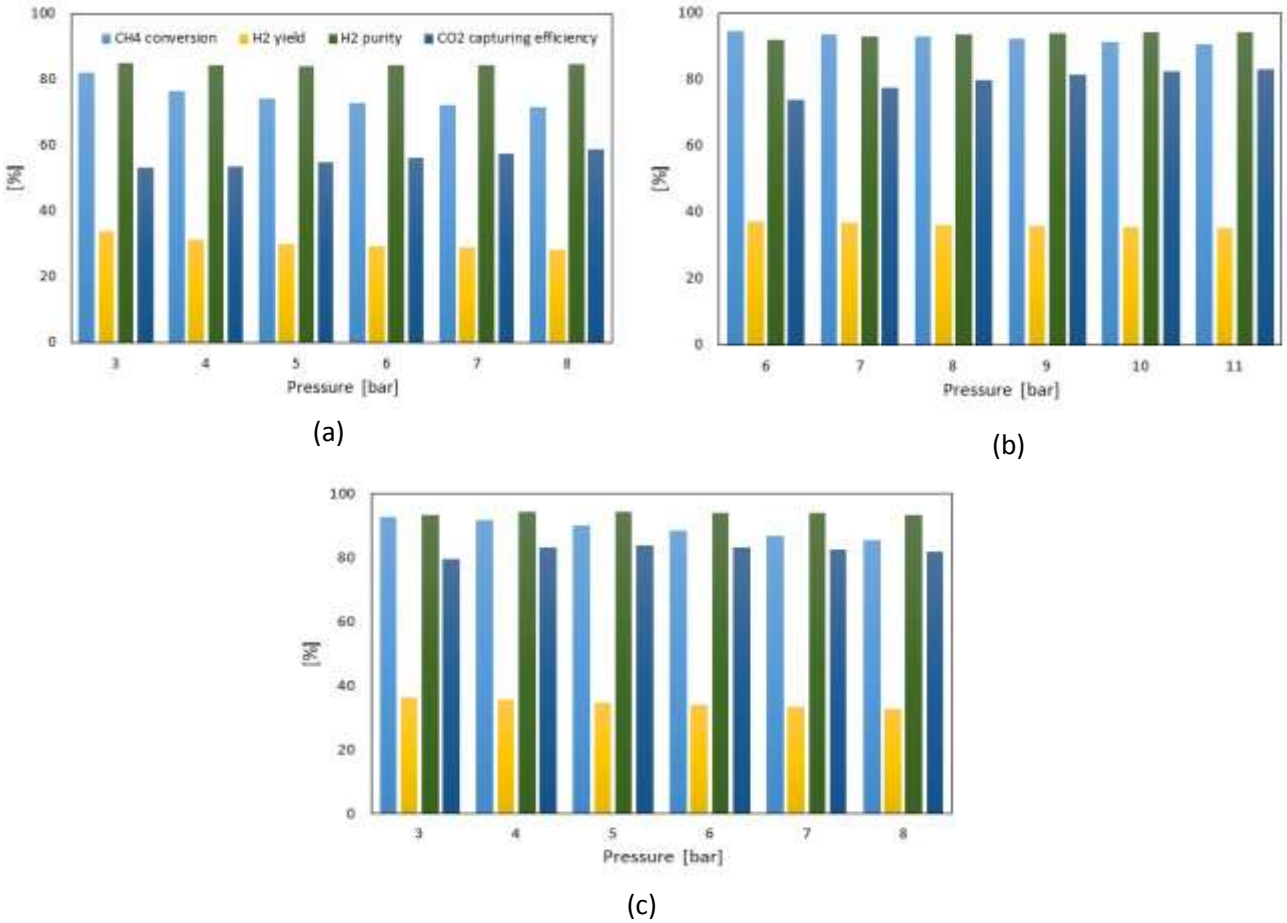

Figure 3.7: The effect of pressure on CH_4 conversion, H_2 yield (wt. % of CH_4), H_2 purity and CO_2 capture efficiency using (a) CaO, (b) LZC and (c) HTC at the optimum temperatures, S/C of 3.0 and sorbent/carbon of 1.

conditions (3 – 11 bar) in terms of CH_4 conversion, H_2 yield (wt. % of CH_4), H_2 purity and CO_2 capture efficiency. Figure 3.7(a) shows the effect of pressure on the performance of SE-SMR process using CaO as sorbent at 900 K, S/C of 3 and G_s of 3.5 kg $m^{-2}s^{-1}$. The pressure has negative effect on the CH_4 conversion and H_2 yield, whereas the CO_2 capture efficiency increases as the pressure increases. Abbas et al. [37] also reported the positive effect of pressure on the carbonation kinetics. This is because the carbonation kinetics used in this model favor relatively high pressure. Using CaO as a sorbent gives 81.98% CH_4 conversion at 3 bar as compared to 71.54% at 8 bar. H_2 purity decreases from 85.02% to 84.15% as pressure increases from 3-4 bar. The decrease in H_2 purity is due to the decrease in CH_4 conversion from 81.98 – 76.56 % as pressure increases from 3 – 4 bar. After 4 bar, H_2 purity almost remains steady due to a slight increase in CO_2 capture efficiency.

CH_4 conversion and H_2 yield for LZC and HTC decreases by increasing the feed pressure because the kinetics of SMR process is not favorable at high pressure. The decrease in CH_4 conversion with the increase in pressure results in decrease in H_2 purity. The LZC sorbent gives maximum CH_4 conversion and H_2 yield up to 94.39% and 37.09% respectively at 6 bar. H_2 purity increases from 91.81 – 94.23% as pressure increases from 6 – 11 bar. The increase in H_2 purity with the increase in pressure is mainly due to the increase in CO_2 capture efficiency. Figure 3.7(c) shows the effect of pressure on SE-SMR process using HTC as a sorbent at 900 K and G_s of 0.5 $kgm^{-2}s^{-1}$. At 3 bar, the CH_4 conversion and H_2 purity achieve is 92.8 % and 93.37 % respectively. As the pressure increases from 3 – 8bar, the CH_4 conversion decreases from 92.8 – 85.51%. In case of HTC, different trend is observed for both H_2 purity and CO_2 capture efficiency, as both approach their peak values at 5 bar. The optimum values of pressure selected for LZC and HTC are 10 bar and 5 bar respectively.

Figure 3.8 (a – c) illustrates the effect of pressure on the rate of reforming (R1) and carbonation reaction for the three sorbents under consideration. The significant impact of pressure is observed on the CO_2 sorption because the rate of carbonation is strongly depended upon pressure conditions as reported by Abbas et al. [2]. In Figure 3.8(a), the effect of pressure on the rate of reforming (r_{SMR}) and carbonation reactions (r_{ads}) using CaO as sorbent is presented. Both r_{ads} and r_{SMR} decrease as the pressure increases from 3 – 6 bar. The r_{SMR} is approximately 4.5 times faster than r_{ads} at 3 bar. The maximum r_{ads} for CaO is found to be 13.6×10^{-4} mol $kg^{-1}s^{-1}$. In Figure 3.8(b), an entirely different trend is observed for LZC as both r_{ads} and r_{SMR} increase as the pressure increases from 9 – 12 bar. The r_{SMR} for LZC is 2.5 times faster than r_{ads}. The r_{ads} for CaO is much faster than LZC and HTC at their optimum pressure conditions, which prove very fast kinetics of CaO as compare to LZC and HTC sorbents. The r_{ads} for HTC is higher at 7 bar than 4 bar, which means more CO_2 capturing is observed at 7 bar as compare to 4 bar. The maximum r_{ads} for HTC at 4 bar occurs at 1550s as compared to 1740s at 7 bar.

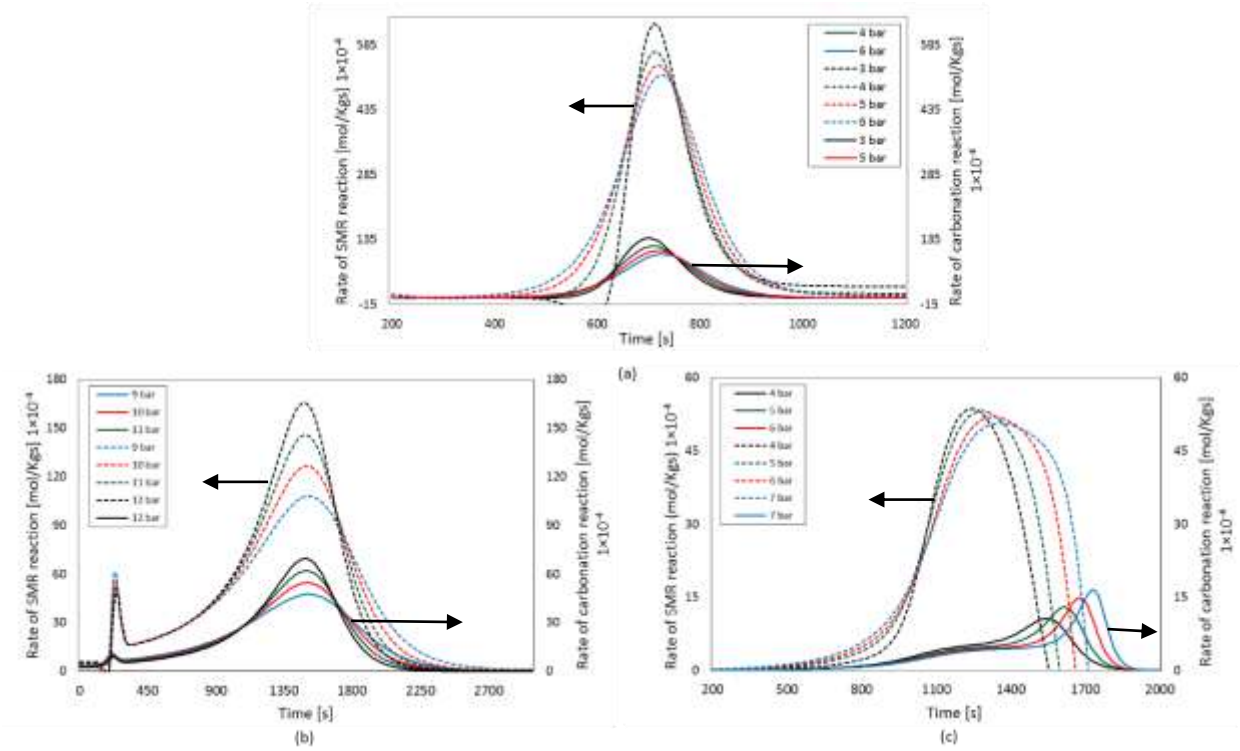

Figure 3.8: The effect of pressure on the rate of SMR reaction (R1) and rate of carbonation by using (a) CaO at 900 K, S/C of 3.0 and G_s of 3.5 $kgm^{-2}s^{-1}$, (b) LZC at T = 950 K, S/C of 3.0 and G_s of 2.5 $kgm^{-2}s^{-1}$ and (c) HTC at 900 K, S/C of 3.0 and G_s of 0.5 $kgm^{-2}s^{-1}$.

3.4.3-Effect of G_s

Gs plays a vital role in the performance of SE-SMR process. The value of G_s dictates the selection of reactor length and cut-off time between sorption and desorption process. The higher values of G_s is favorable for shorter reactor length and fast cycling operations i.e. sorption and desorption. Figure 3.9 (a – c) shows the effect of G_s on H_2 and CO_2 composition (mole %, dry basis) at the outlet of the reactor for CaO, LZC and HTC sorbents.

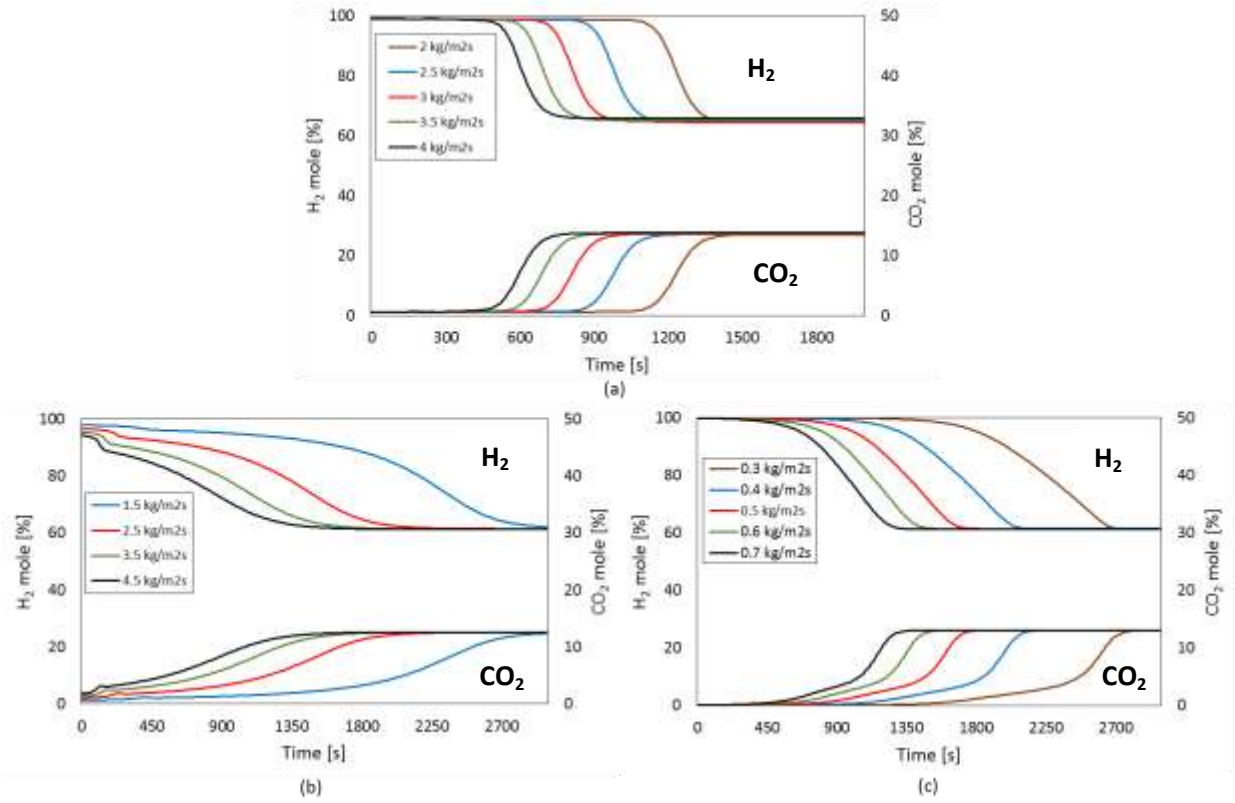

Figure 3.9: The effect of G_s on the H_2 and CO_2 molar composition (dry basis) by using (a) CaO at 900 K, S/C of 3.0 and 3 bar, (b) LZC at 950 K, S/C of 3.0 and 10 bar and (c) HTC at 900 K, S/C of 3.0 and 5 bar.

Figure 3.9(a) shows the variation in CO_2 and H_2 composition during SE-SMR process using CaO sorbent at 900 K, 3 bar and S/C of 3. At low G_s, (2 $kgm^{-2}s^{-1}$), longer pre-breakthrough is observed (t = 1150s). In Figure 3.9(b), similar trend is observed using LZC sorbent. With the increase in G_s, pre-breakthrough period decreases with no significant effect on the molar composition of H_2 and CO_2 at the outlet of the reactor. In case of CaO as sorbent, the pre-breakthrough period decreases from 1150 – 550 s as G_s increases from 2 $kgm^{-2}s^{-1}$ to 4 $kgm^{-2}s^{-1}$. The G_s of 3.5 $kgm^{-2}s^{-1}$ is selected as optimum velocity for CaO sorbent and this gives 81.98% and 85.02% CH_4 conversion and H_2 purity respectively.

Figure 3.9(c) shows a significant change in the pre-breakthrough curve in case of HTC sorbent. The pre-breakthrough changes from 990 – 1690 s as G_s varies from 0.7 $kgm^{-2}s^{-1}$ to 0.5 $kgm^{-2}s^{-1}$.

Here, considerable change is also observed in CH_4 conversion and H_2 purity by changing the G_s. This change is not prominent in case of CaO as the kinetics of CaO sorbent is fast and not effected much by changing the G_s. The kinetics of HTC sorbent is slow, which means long residence time is required to achieve high CH_4 conversion and H_2 purity. That is why, the optimum for HTC (0.5 $kgm^{-2}s^{-1}$) is 7 times smaller than the G_s selected for CaO (3.5 $kgm^{-2}s^{-1}$).

3.4.4-CH_4 conversion enhancement factor (C_F)

The C_F explains how much CH_4 conversion is increased by using SE-SMR processes as compare to the CH_4 conversion in conventional SMR process. It is used to identify the performance of the sorbents. The C_F decreases as the sorbent bed approaches its saturation point. The enhancement in CH_4 is mainly due to the rise in temperature in SE-SMR process, which favors endothermic reforming reactions R1 and R2. Secondly, the sorbent decreases partial pressure of CO_2 by removing it from the product gas and this results in shifting chemical equilibrium of reforming reactions R1 and R2 towards more CH_4 conversion. The C_F is calculated as;

$$C_F = \frac{(X_{CH4})_{ad} - (X_{CH4})_{nad}}{(X_{CH4})_{nad}} \times 100 \quad (7)$$

Table 3.2 shows the effect of S/C on C_F for the three sorbents used in this study. CaO gives 40.4% C_F at S/C of 1. By increasing S/C from 1 – 2, C_F also increases from 40.4 – 71.9%. The sudden increase in C_F is because the steam is introduced from its sub-stoichiometric amount (S/C = 1) to the stoichiometric amount (S/C = 2). The further increase in S/C from 3 – 4 decreases the C_F from 67% - 52.9%. Since stoichiometric conditions are not favorable for CH_4 conversion, and H_2 purity, so S/C of 3 is selected in this work as optimum value for all three sorbents. Also, generation of high S/C requires more heat, so the thermal efficiency of the overall process would decrease. LZC and HTC shows similar trend but they give more C_F than CaO because they operate at relatively higher pressures as the use of relatively high pressures than CaO suppresses $X_{CH4,nad}$. The C_F of 110.8% and 118 % is obtained at S/C of 3 using LZC and HTC respectively.

Table 3.2: The effect of S/C on C_F using different sorbents

	CH_4 Conversion Enhancement (C_F)		
S/C	**CaO**	**LZC**	**HTC**
1	40.4	71.6	107.8
2	71.9	118.6	146.2
3	67.0	110.8	118.0
4	52.9	83.0	96.4

3.5-Comparison of sorbent capacities

The sorption kinetics is another performance parameter considered in the choice of sorbent. The fast kinetic is preferred along with high H_2 purity and CH_4 conversion. Figure 3.10 shows the adsorb concentration ($molkg^{-1}$) of CO_2 with time along the length of reactor by using CaO, LZC and HTC sorbents. Figure 3.10(a) shows the dynamic profile of CO_2 sorption over CaO. The sorption curve moves along the length of reactor at a rate of 0.013 mol_{CO2} kg^{-1} s^{-1}. The sharp curve at the start of the reactor (L = 1m) shows the rapid sorption of CO_2. The time rate of change of CO_2 sorption over CaO sorbent is almost steady as the CO_2 passes over the reactor bed length. Figure 3.10 (b and c) shows the variation of sorption curves along the length of the reactor using LZC and HTC respectively.

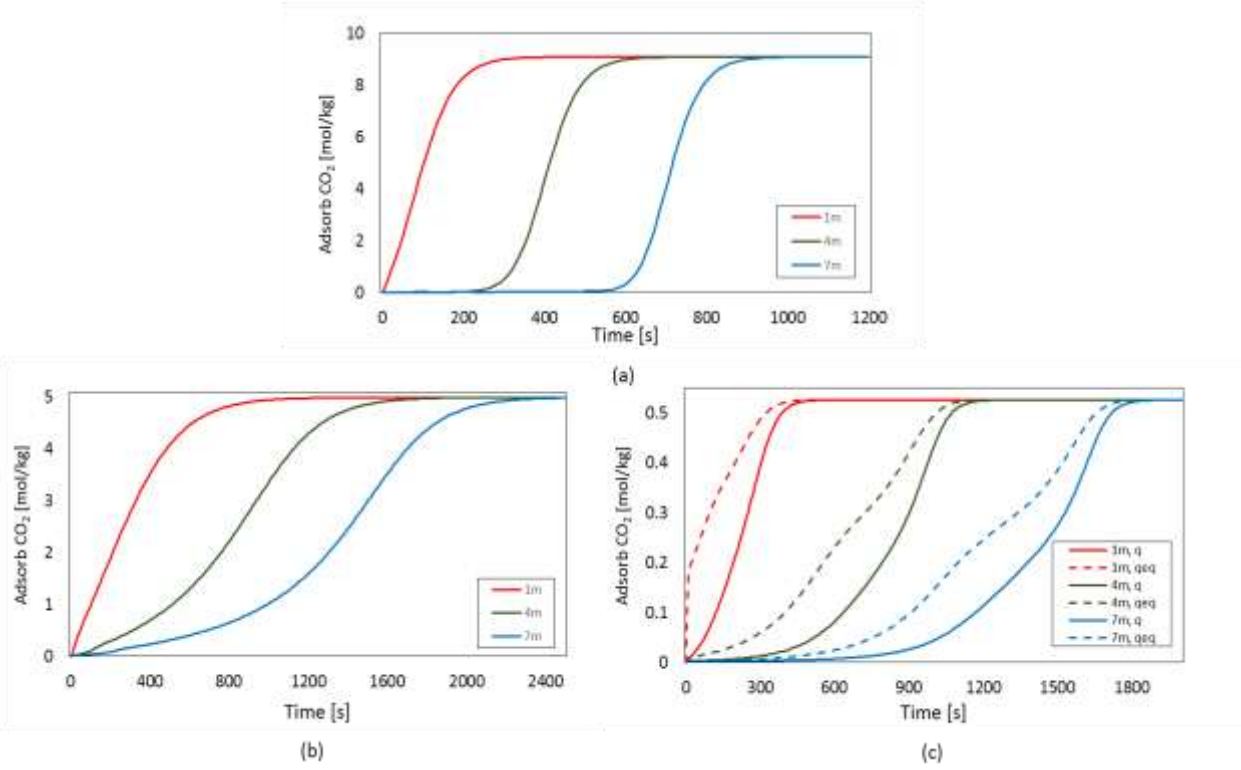

Figure 3.10: CO_2 adsorb concentration using (a) CaO at 900 K, S/C of 3.0, 3 bar and Gs of 3.5 $kgm^{-2}s^{-1}$, (b) LZC at 950 K, S/C of 3.0,10 bar, and Gs of 2.5 $kgm^{-2}s^{-1}$ and (c) HTC at 900 K, S/C of 3.0, 5 bar and Gs of 0.5 $kgm^{-2}s^{-1}$.

For LZC and HTC, a sharp peak at the start of the reactor is observed. This is due to the availability of high amount of CO_2 at the start of the reactor. The maximum rate of sorption at the outlet of the reactor using LZC and HTC is 0.0054 mol_{CO2} kg^{-1} s^{-1} and 0.0012 mol_{CO2} kg^{-1} s^{-1} respectively. The low value of CO_2 sorption on HTC as compare to CaO (9 mol_{CO2} kg^{-1} s^{-1}) and LZC (5 mol_{CO2} kg^{-1} s^{-1}) is due to the low sorption capacity (m_{CO2} =0.65 mol_{CO2} kg^{-1} s^{-1}) of HTC. The r_{ads} of HTC is approximately 10 times slow than the r_{ads} of CaO at their optimum conditions.

Chapter 4 CONCLUSIONS

The performance of SMR process can be significantly improved by using sorbents along with the catalyst during the SMR process. There are many sorbents available that could adsorb CO_2 at high temperatures. The choice of these sorbents normally depends upon the CO_2 capture kinetics and sorbent capacity. The present mathematical model is capable of illustrating the performance of SE-SMR process in terms of CH_4 conversion, H_2 purity, H_2 yield (wt. % of CH_4) and CO_2 capture efficiency. A rise in temperature, during the pre-breakthrough period, is observed using LZC and CaO sorbents and on the other hand HTC shows no rise in in temperature during the pre-breakthrough period. The highly endothermic nature of SE-SMR process, using HTC ($\Delta H^0_{298K} = 191\ kJmol^{-1}_{CH4}$), restricts the rise in temperature during the pre-breakthrough period. ΔT_{rise} for CaO and LZC is found to be 17.5 K and 20K respectively. This shows the highly exothermic nature of these sorbents. A pre-breakthrough period of 690s, 250s and 1040s is observed using CaO LZC and HTC respectively. The optimum pressure and temperature conditions obtain for CaO is 3 bar and 900 K respectively. The temperature higher than 900 K for CaO causes decline in H_2 purity and CO_2 capturing efficiency whereas, high pressure gives low CH_4 conversion. The choice of S/C depends on the overall operational cost of the plant. The S/C higher than 2 would increase the steam production cost. Also, high S/C increases CH_4 conversion and CO_2 capturing efficiency. So, there is always a tradeoff between CH_4 conversion and overall operational cost of the plant in selecting the S/C. The selection of G_s depends on the operational time of the SE-SMR reactor. The optimum S/C and G_s selected using CaO is 3.0 and 3.5 $kgm^{-2}s^{-1}$ respectively. The LZC gives more CH_4 conversion than CaO at 10 bar, 950 K, S/C of 3.0 and 2.5 $kgm^{-2}s^{-1}$. The CO_2 capturing efficiency increases with pressure using LZC, but at very high pressures, the CH_4 conversion decreases quickly. The optimum values for HTC are found to be 900 K, 5 bar, S/C of 3 and 0.5 $kgm^{-2}s^{-1}$. The conversion enhancement factor (C_F) decreases with the increase in S/C from 2 – 4. The C_F for CaO, LZC and HTC is found to be 76%, 110.8% and 118.0% respectively at S/C of 3. Overall, LZC and HTC are good in terms of high CH_4 conversion, H_2 purity and yield and CO_2 capturing efficiency than CaO. But, CaO possess fast CO_2 capture kinetics than LZC and HTC. The sorbent capacity of CaO is also much higher than LZC (approx. 2 times) and HTC (approx. 18 times).

References:

[1] R. B. Gupta, *HYDROGEN FUEL Production, Transport, and Storage*. CRC Press, 2009.

[2] S. Z. Abbas, V. Dupont, and T. Mahmud, "ScienceDirect Modelling of H 2 production in a packed bed reactor via sorption enhanced steam methane reforming process," *Int. J. Hydrogen Energy*, vol. 42, no. 30, pp. 18910–18921, 2017.

[3] J. R. Fernandez, J. C. Abanades, and R. Murillo, "Modeling of sorption enhanced steam methane reforming in an adiabatic fixed bed reactor," *Chem. Eng. Sci.*, vol. 84, pp. 1–11, 2012.

[4] H. K. Rusten, E. Ochoa-Fernández, D. Chen, and H. A. Jakobsen, "Numerical investigation of sorption enhanced steam methane reforming using \ce{Li2ZrO3} as \ce{CO2}-acceptor," *Ind. Eng. Chem. Res.*, vol. 46, no. 13, pp. 4435–4443, 2007.

[5] J. P. Jakobsen and E. Halmøy, "Energy Procedia Reactor Modeling of Sorption Enhanced Steam Methane Reforming," *Energy Procedia*, vol. 1, no. 1, pp. 725–732, 2009.

[6] D. P. Harrison, "Sorption-Enhanced Hydrogen Production : A Review," pp. 6486–6501, 2008.

[7] L. Ã. Barelli, G. Bidini, F. Gallorini, and S. Servili, "Hydrogen production through sorption-enhanced steam methane reforming and membrane technology : A review," vol. 33, pp. 554–570, 2008.

[8] J. M. Silva, R. Trujillano, V. Rives, M. A. Soria, and L. M. Madeira, "High temperature CO 2 sorption over modified hydrotalcites," *Chem. Eng. J.*, vol. 325, pp. 25–34, 2017.

[9] A. L. García-lario, G. S. Grasa, and R. Murillo, "Performance of a combined CaO-based sorbent and catalyst on H 2 production , via sorption enhanced methane steam reforming," vol. 264, pp. 697–705, 2015.

[10] J. R. Hufton, S. Mayorga, and S. Sircar, "Sorption-Enhanced Reaction Process for Hydrogen Production," vol. 45, no. 2, 1999.

[11] B. Balasubramanian, A. L. Ortiz, S. Kaytakoglu, and D. P. Harrison, "Hydrogen from methane in a single-step process," vol. 54, pp. 3543–3552, 1999.

[12] K. B. Yi and D. P. Harrison, "KINETICS , CATALYSIS , AND REACTION ENGINEERING Low-Pressure Sorption-Enhanced Hydrogen Production," pp. 1665–1669, 2005.

[13] B. Arstad, J. Prostak, and R. Blom, "Continuous hydrogen production by sorption enhanced steam methane reforming (SE-SMR) in a circulating fluidized bed reactor : Sorbent to catalyst ratio dependencies," *Chem. Eng. J.*, vol. 189–190, pp. 413–421, 2012.

[14] K. Johnsen, J. R. Grace, S. S. E. H. Elnashaie, L. Kolbeinsen, and D. Eriksen, "Modeling of Sorption-Enhanced Steam Reforming in a Dual Fluidized Bubbling Bed Reactor," pp. 4133–4144, 2006.

[15] Y. Huang, S. Rebennack, and Q. P. Zheng, "Techno-economic analysis and optimization models for carbon capture and storage : a survey," 2013.

[16] Y. Ding and E. Alpay, “Equilibria and kinetics of CO adsorption on hydrotalcite adsorbent,” vol. 55, pp. 3461–3474, 2000.

[17] K. D. Binay, “Principles of Mass Transfer and Separation Process.” .

[18] E. Ochoa-ferna, G. Haugen, T. Zhao, M. Rønning, I. Aartun, and B. Børresen, “Process design simulation of H 2 production by sorption enhanced steam methane reforming : evaluation of potential CO 2 acceptors {,” pp. 654–662, 2007.

[19] S. Kumar and S. K. Saxena, “A comparative study of CO 2 sorption properties for different oxides,” 2014.

[20] M. S. Yancheshmeh, H. R. Radfarnia, and M. C. Iliuta, “High temperature CO 2 sorbents and their application for hydrogen production by sorption enhanced steam reforming process,” *Chem. Eng. J.*, vol. 283, pp. 420–444, 2016.

[21] W. Roger, “HYDROGEN PRODUCTION,” pp. 1–4, 1933.

[22] D. Ki, I. Hyun, and W. Lai, “Modeling and simulation for the methane steam reforming enhanced by in situ CO 2 removal utilizing the CaO carbonation for H 2 production,” vol. 59, pp. 931–942, 2004.

[23] C. Han and D. P. Harrison, “Simultaneous shift reaction and carbon dioxide separation for the direct production of hydrogen,” *Chem. Eng. Sci.*, vol. 49, no. 24, pp. 5875–5883, 1994.

[24] Z. Zhou, Y. Qi, M. Xie, Z. Cheng, and W. Yuan, “Synthesis of CaO-based sorbents through incorporation of alumina / aluminate and their CO 2 capture performance,” *Chem. Eng. Sci.*, vol. 74, pp. 172–180, 2012.

[25] M. Xie, Z. Zhou, Y. Qi, Z. Cheng, and W. Yuan, “Sorption-enhanced steam methane reforming by in situ CO 2 capture on a CaO – Ca 9 Al 6 O 18 sorbent,” *Chem. Eng. J.*, vol. 207–208, pp. 142–150, 2012.

[26] H. K. Rusten, *Hans Kristian Rusten Simulation and modelling of hydrogen production by sorption enhanced steam methane reforming in fixed bed reactors Hans Kristian Rusten Simulation and modelling of hydrogen production by sorption enhanced steam methane reforming in fi*. 2010.

[27] M. H. Halabi, M. H. J. M. De Croon, J. Van Der Schaaf, P. D. Cobden, and J. C. Schouten, “Reactor modeling of sorption-enhanced autothermal reforming of methane . Part I : Performance study of hydrotalcite and lithium zirconate-based processes,” *Chem. Eng. J.*, vol. 168, no. 2, pp. 872–882, 2011.

[28] Y. Ding and E. Alpay, “Adsorption-enhanced steam } methane reforming,” vol. 55, pp. 3929–3940, 2000.

[29] A. Hanif, S. Dasgupta, S. Divekar, A. Arya, M. O. Garg, and A. Nanoti, “A study on high temperature CO 2 capture by improved hydrotalcite sorbents,” *Chem. Eng. J.*, vol. 236, pp. 91–99, 2014.

[30] M. H. Halabi, M. H. J. M. De Croon, J. Van Der Schaaf, P. D. Cobden, and J. C. Schouten, “Kinetic and structural requirements for a CO 2 adsorbent in sorption enhanced

catalytic reforming of methane – Part I : Reaction kinetics and sorbent capacity," *Fuel*, vol. 99, pp. 154–164, 2012.

[31] H. K. Rusten, H. A. Jakobsen, E. Ochoa-ferna, M. Rønning, A. Holmen, and D. Chen, "Sorption enhanced hydrogen production by steam methane reforming using Li 2 ZrO 3 as sorbent : Sorption kinetics and reactor simulation," vol. 106, pp. 41–46, 2005.

[32] J. G. Xu and G. F. Froment, "Methane Steam Reforming, Methanation and Water-Gas Shift .1. Intrinsic Kinetics," *Aiche J.*, vol. 35, no. 1, pp. 88–96, 1989.

[33] I. Aloisi, N. Jand, S. Stendardo, and P. Ugo, "Hydrogen by sorption enhanced methane reforming : A grain model to study the behavior of bi-functional sorbent-catalyst particles," *Chem. Eng. Sci.*, vol. 149, pp. 22–34, 2016.

[34] V. Nikulshina and A. Steinfeld, "Kinetic analysis of the carbonation reactions for the capture of CO 2 from air via the Ca (OH) 2 – CaCO 3 – CaO solar thermochemical cycle," vol. 129, pp. 75–83, 2007.

[35] M. Alonso, J. C. Abanades, and N. Rodrı, "Experimental Investigation of a Circulating Fluidized-Bed Reactor to Capture CO 2 with CaO," vol. 57, no. 5, 2011.

[36] R. Xiong, J. Ida, and Y. S. Lin, "Kinetics of carbon dioxide sorption on potassium-doped lithium zirconate," vol. 58, pp. 4377–4385, 2003.

[37] S. Z. Abbas, V. Dupont, and T. Mahmud, "ScienceDirect Kinetics study and modelling of steam methane reforming process over a NiO / Al 2 O 3 catalyst in an adiabatic packed bed reactor," *Int. J. Hydrogen Energy*, vol. 42, no. 5, pp. 2889–2903, 2016.

[38] D. Chattaraj, "Structural , electronic , elastic and thermodynamic properties of Li 2 ZrO 3 : A comprehensive study using DFT formalism," *J. Nucl. Mater.*, vol. 496, pp. 286–292, 2017.

[39] "The heat capacities and derived t h e r m o p h y s i c a l properties of LizZrO 3 and LisZrO e at temperatures f r o m 0 to 1000 K," vol. 0, pp. 1251–1256, 1992.

Appendix A: SMR and sorbent kinetic data

A1: The SMR kinetic data along with kinetic rate constants and equilibrium constants;

$$R_1 = \frac{k_1}{p_{H_2}^{2.5}}\left(p_{CH_4}p_{H_2O} - \frac{p_{H_2}^3 p_{CO}}{K_I}\right)\left(\frac{1}{\Omega^2}\right) \qquad (A1-1)$$

$$R_2 = \frac{k_2}{p_{H_2}}p_{CO}p_{H_2O} - \frac{p_{H_2}p_{CO_2}}{K_{III}}\left(\frac{1}{\Omega^2}\right) \qquad (A1-2)$$

$$R_3 = \frac{k_3}{p_{H_2}^{3.5}}\left(p_{CH_4}p_{H_2O}^2 - \frac{p_{H_2}^4 p_{CO_2}}{K_{II}}\right)\left(\frac{1}{\Omega^2}\right) \qquad (A1-3)$$

R_1 is the rate expression for SMR reaction (R1)

R_2 is the rate expression for SMR reaction (R2)

R_3 is the rate expression for WGS reaction (R3)

k_1, k_2 and k_3 are the reaction rate constants for reactions R1, R2 and R3 respectively

$$k_1 = k_{0,1}\exp\left(\frac{-E_1}{RT}\right) = (1.17 \times 10^{15})\exp\left(\frac{-240100}{RT}\right) \qquad (A1-4)$$

$$k_2 = k_{0,2}\exp\left(\frac{-E_2}{RT}\right) = (5.43 \times 10^{5})\exp\left(\frac{-67130}{RT}\right) \qquad (A1-5)$$

$$k_3 = k_{0,3}\exp\left(\frac{-E_3}{RT}\right) = (2.83 \times 10^{14})\exp\left(\frac{-243900}{RT}\right) \qquad (A1-6)$$

$$K_I = \exp\left(\frac{-26830}{T_s} + 30.114\right) \qquad (A1-7)$$

$$K_{II} = \exp\left(\frac{4400}{T_s} - 4.036\right) \qquad (A1-8)$$

$$K_{III} = K_I K_{II} \qquad (A1-9)$$

Kj = thermodynamic equilibrium constant for SMR reactions.

$$\Omega = 1 + K_{CO}p_{CO} + K_{H_2}p_{H_2} + K_{CH_4}p_{CH_4} + K_{H_2O}\frac{p_{H_2O}}{p_{H_2}} \qquad (A1-10)$$

$$K_i = K_{oi}\exp\left(\frac{-\Delta H_i}{R_g T}\right) \qquad (A1-11)$$

Ki = sorption constant for component gaseous 'i'

A2: Rate equation of CaO sorbent

$$\frac{dq_{CO2}}{dt} = k_{carb}(X_{max} - X)(\upsilon_{CO2} - \upsilon_{CO2,eq}) \times {}^{1000}/_{56} \qquad (A2-1)$$

Where, q_{CO2}[$mol_{CO2}/kg_{sorbent}$ is the molar concentration of CO_2 adsorb per kg of sorbent. $\upsilon_{CO2,eq}$ is the volumetic fraction of CO_2 at equilibrium conditions.
X_{max} (maximum carbonation conversion) = 0.4
k_{carb} (rate of carbonation) = 0.35 s^{-1}

$$\upsilon_{CO2,eq} = (4.137 \times 10^7)\exp\left(\frac{-20474}{T}\right) \qquad (A2-2)$$

Maximum carbonation conversion (X_{max}) is given as

$$X_{max} = 96.34\exp\left(\frac{-12171}{T}\right)4.49\exp\left(\frac{4790.6}{T}\right) \qquad (A2-3)$$

A4: HTC sorbent kinetic model

$$r_{ads} = \frac{\partial q_{CO_2}}{\partial t} = k_{carb}(q^*_{CO_2} - q_{CO_2}) \qquad (A4\text{-}1)$$

Where, 'q_{CO_2}' is the equilibrium CO_2 concentration on sorbent, ($mol_{CO2}Kg^{-1}{}_{sorbent}$)

$$k_{carb} = \frac{15}{r_p^2}\frac{\epsilon_p D_p}{\epsilon_p + (1-\epsilon_p)\rho_p RT\left(\frac{\partial q^*_{CO_2}}{\partial p_{CO_2}}\right)} \qquad (A4\text{-}2)$$

Where, 'k_{CO_2}' is the sorption constant,
'D_p' is the pore diffusion coefficient, with 1.1×10^{-6} m^2s^{-1}

$$q^*_{CO_2} = \frac{m_{CO_2} b_{CO_2} p_{CO_2}}{1 + b_{CO_2} p_{CO_2}} \qquad (A4\text{-}3)$$

Where, p_{CO_2} = Partial pressure of CO_2 in the gas phase
m_{CO_2} (maximum sorption capacity of HTC) = 0.65 $mol_{CO2}Kg^{-1}{}_{sorbent}$
The temperature dependent Langmuir parameter (b_{CO_2}) is given as;

$$b_{CO_2} = b_{CO_2,ref}\exp\left[-\frac{\Delta H_{ads}}{R}\right]\left(\frac{1}{T} - \frac{1}{T_o}\right) \qquad (A4\text{-}4)$$

Where, ΔH_{ads} (Heat of sorption) = -17kJmol^{-1}

$b_{CO_2,ref}$ = 23.6×10^{-2} kPa^{-1}
T_o (reference temperature for b_{CO_2}) = 673 K

A3: CO_2 sorption kinetics of LZC

$$\frac{dx}{dt} = k_{carb} C_{CO_2}^{n} (1 - x) \quad \text{(A3-1)}$$

Where, x = extent of reaction. It is defined as x = $\frac{q_{CO_2}}{q_{CO_2,max}}$ .The maximum uptake of CO_2 ($q_{CO_2,max}$) experimentally (reported by Fernendez et al.) is 5.0 $mol_{CO2}Kg^{-1}_{sorbent}$
k_{carb} = 4.9 × 10–5 $m^{3n}/mol^{n}s$ (sorption rate constant)
n = 0.93 (order of sorption reaction)

$$r_{ads} = \frac{q_{CO_2,max}}{m_{CO_2}} \frac{dx}{dt} \quad \text{(A3-2)}$$

$$k_{carb} = k_{carb}^{o} \exp\left[-\frac{E_{ad}}{R}\left(\frac{1}{T} - \frac{1}{T_o}\right)\right] \quad \text{(A3-3)}$$

E_{ad} (activation energy) = 8.94 × 10^4 Jmol^{-1}
T_o = 673 K

Appendix-B Empirical correlations

B1 Empirical correlations

$$D_z = 0.73 D_m + \frac{0.5 u_s d_p}{1 + \frac{9.49 D_m}{u_s d_p}} \quad (B1-1)$$

Where, D_z is the axial dispersion coefficient, (m^{2}s^{-1})
D_m is the molecular diffusivity, (m^{2}s^{-1})
The thermal conductivity(Wm^{-1}K^{-1}) and mass transfer coefficient (m^{3}m^{-2}s^{-1}) is given as;

$$\frac{\lambda_z^f}{\lambda_g} = \frac{\lambda_z^o}{\lambda_g} + 0.75 Pr Re_p \quad (B1-2)$$

$$\frac{\lambda_z^o}{\lambda_g} = \varepsilon_b + \frac{1 - \varepsilon_b}{0.139\varepsilon_b - 0.0339 + \frac{\left(\frac{2}{3}\right)\lambda_g}{\lambda_s}} \quad (B1-3)$$

$$k_{g,i} = j_{D,i} Re Sc_i^{\frac{1}{3}} \frac{D_i}{d_p} \qquad (B1-4)$$

$$\varepsilon_b j_{D,i} = 0.765 Re^{-0.82} + 0.365 Sc_i^{-0.398} \qquad (B1-5)$$

Dimensionless numbers used in this study is shown by the following relationship

$$Re = \frac{\rho_f u_s d_p}{\mu} \quad ; \quad 0.01 < Re < 1500 \qquad (B1-6)$$

$$Sc_i = \frac{\mu}{\rho_f D_i} \quad ; \quad 0.6 < Sc < 7000 \ , \ 0.25 < \varepsilon_b < 0.96 \qquad (B1-7)$$

$$Pr = \frac{C_{pg}\mu_g}{\lambda_g} \qquad (B1-8)$$

Heat transfer coefficient (h_f) with its dimensionless number (j_H)is given as

$$h_f = j_H \frac{C_{pg} G_s}{Pr^{\frac{2}{3}}} \qquad (B1-9)$$

$$j_H = 0.91 Re^{-0.51} \psi \quad ; \quad 0.01 < Re < 50 \qquad (B1-10)$$

$$j_H = 0.61 Re^{-0.41} \psi \quad ; \quad 50 < Re < 1000 \qquad (B1-11)$$

Appendix C: Rate equations for component 'i'

C-1 The rate of formation or consumption of component 'i' is given as;

$$r_i = \sum_{j=1}^{3} \eta_i \varphi_{ij} R_j \qquad i = CH_4, CO, CO_2, H_2 \text{ and } H_2O \qquad (6)$$

For all component, it is given as;

$$r_{CH_4} = -R_1 - R_2 \qquad (6-a)$$
$$r_{H_2O} = -R_1 - 2R_2 - R_3 \qquad (6-b)$$
$$r_{H_2} = 3R_1 + 4R_2 + R_3 \qquad (6-c)$$
$$r_{CO_2} = R_2 + R_3 \qquad (6-d)$$
$$r_{CO} = R_1 - R_3 \qquad (6-7)$$

where, φ_{ij} is the stoichiometric coefficient. The value of φ_{ij} is negative for reactants and positive for products.